0305014

P

RAPPORT

Magnetic Resonance Imaging of Wood at its Interface with Glue Coatings and Air

Final report to EC

MARWINGCA

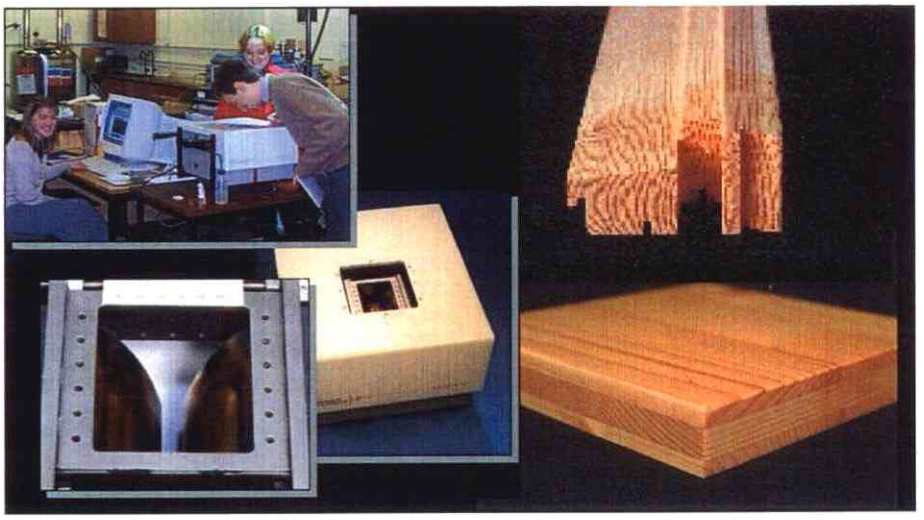

Trätek

INSTITUTET FÖR TRÄTEKNISK FORSKNING

Henrik Berglind, Jan Ekstedt, Anders Rosenkilde, Jarl-Gunnar Salin – Trätek
Peter J. McDonald, Graham Bennett, Joseph L. Keddie – University of Surrey
Guntis Brands, Pentti Jokinen – WSAB-Puutavakuivaamot OY

MAGNETIC RESONANCE IMAGING OF WOOD AT ITS INTERFACE WITH GLUE COATINGS AND AIR

Final report to EC contract number QLK5 1999 01587 MARWINGCA

Trätek, Rapport P 0305014

ISSN 1102 – 1071
ISRN TRÄTEK – R – – 03/014 – – SE

Keywords

coatings
drying
glues
NMR
MRI

UniS University of Surrey

Trätek

WSAB

Stockholm maj 2003

Rapporter från Trätek – Institutet för träteknisk forskning – är kompletta sammanställningar av forskningsresultat eller översikter, utvecklingar och studier. Publicerade rapporter betecknas med I eller P och numreras tillsammans med alla utgåvor från Trätek i löpande följd.

Reports issued by the Swedish Institute for Wood Technology Research comprise complete accounts for research results, or summaries, surveys and studies. Published reports bear the designation I or P and are numbered in consecutive order together with all the other publications from the Institute.

Trätek – Institutet för träteknisk forskning – betjänar sågverk, trämanufaktur (snickeri-, trähus-, möbel- och övrig träförädlande industri), skivtillverkare och byggindustri.

Institutet är ett icke vinstdrivande bolag med industriella och institutionella kunder. FoU-projekt genomförs både som konfidentiella uppdrag för enskilda företagskunder och som gemensamma projekt för grupper av företag eller för den gemensamma branschen. Arbetet utförs med egna, samverkande och externa resurser. Trätek har forskningsenheter i Stockholm, Växjö och Skellefteå.

The Swedish Institute for Wood Technology Research serves sawmills, manufacturing (joinery, wooden houses, furniture and other woodworking plants), board manufacturers and building industry.

The institute is a non-profit company with industrial and institutional customers. R & D projekcts are performed as contract work for individual industrial customers as well as joint ventures on an industrial branch level. The Institute utilises its own resources as well as those of its collaborators and outside bodies. Our research units are located in Stockholm, Växjö and Skellefteå.

Abstract

Magnetic resonance profiling using a recently developed permanent magnet with a strong, tailored field gradient has been used to study wood and its interface with air, coatings and glues.

The study of the wood-air interface is driven by the need to better understand and control the drying of wood. Experimental results presented in the literature clearly indicate that mass transfer from wood surfaces is much slower than predicted by the classical description of drying processes. This is the case both for green softwood sapwood far above the fibre saturation point (FSP) and for wood entirely below FSP. The experiments show that a thin "dry shell" is rapidly formed at the surface as the free water withdraws in the form of a receding evaporation front. However, previous to this study there has been no direct visualisation of water concentrations in the dry shell with sufficient spatial and temporal resolution to enable assessment of quantitative modelling.

The magnetic resonance results presented in Part I of this report provide this data. The results show the moisture profile within the outer part of this "dry shell" with a resolution of 13 to 21 μm. The surface of the wood has a much lower moisture content than indicated by the extrapolation of the profile in the bulk of the wood sample to the surface. It has been proposed that slow mass transfer below the FSP is due to a dynamic non-equilibrium between the gaseous and the bound water phase. Thus the relative humidity in the air close to the surface is lower (in desorption) that predicted for wood in equilibrium.

The study of the wood-coatings interface is driven by a need to better understand the interaction of aqueous coatings with wood. These more environmentally friendly coatings are increasingly demanded by environmental legislation compared to their solvent borne counterparts. However questions remain as to their efficacy in preventing moisture transport across the interface and about the effect of surfactant migration on the equilibrium moisture levels in the wood immediately below the coating. These questions are important for considerations of durability. The study of the wood-glue interface is likewise driven by a need to better understand the glue-wood interaction, the curing of the glue and the efficacy of the glue line as a water barrier.

In Part II the drying above phenomena are discussed in more detail. Theoretical calculations are performed based on previously published experimental data. Finally the possibilities to theoretically predict the dry shell thickness development and its dependence on drying are discussed.

Part III explains how the previous results of Parts I and II are used to develop a new wireless moisture sensor with the possibility to be incorporated in a new kiln control system that involves modelling of the drying process. A large part of the work is focused on how to incorporate the model from Part II, itself based on laboratory measurements in Part I into the new kiln control system. The report discusses the controlling strategy which should be used.

The new wireless sensor is ready and available on the market. Because it is wireless it is very easy to use in larger kilns and also in progressive kilns were the timber is moved from position to position during the whole drying period.

The system has been tested in the laboratory and at a test site in the field. It is now available on the market. Since the system uses a model for simulation of the drying process the control strategy has changed dramatically compared to previous versions of the kiln control system. The new system opens up the possibility of optimising the industrial drying process for improved wood quality, capacity, energy consumption and environmental aspects.

Index

Part I

Developments in Magnetic Resonance Imaging and its application to wood-air, wood-coating and wood-glue interfaces

1 Introduction

This programme of work contributes directly to KEY ACTION 5.3 of the "Quality of life and management of living resources" within the EC 5th Framework programmes. The problems that are addressed through this project relate to wood drying, to water-borne coatings for wood and to loss of structural integrity in glued wood products. In order to give wood products the high quality necessary, these crucial processes of drying, gluing and coating need to be refined. This may be achieved by improving the drying efficacy and the formulation and testing of water-borne coatings and adhesives, thus making the processes and the products of this rural-based, basically traditional but environmentally aware industry more competitive. This project specifically deals with enabling the wood industry to be increasingly competitive by adding value and quality to products and being able to respond to environmental concerns. It contributes to sustainable rural development by improving the tools and products required to process the product accurately, providing the consumer and producer with an added-value product. These problems are addressed using a magnetic resonance profiling with a novel magnet design known as GARField. In every case, GARField is able to measure the water distribution in the interface layers of the wood to provide direct visualisation of moisture transport and build-up as a function of space and time. This enables quantitative assessment of the problems and can lead directly to improved processes and products. In particular, in this project, the results lead to improved models and sensor equipment for kiln drying.

1.1 Wood drying

Wood may be dried to the wrong level because kiln control does not take correct account of the particular parameters of the wood or knowledge of the drying mechanism. This is particularly likely in the case of high value or unusually shaped wood products, for example. The moisture gradients remaining within the wood can cause the material to be rejected due to warping or during subsequent processing.

1.2 Coatings

The moisture layer build-up in wood behind water-borne and low VOC coatings leads to poor durability and reduced product lifetime. This is a function of coating permeability, wood permeability and coating components – in particular the presence of surfactants. This moisture build-up is the single most significant drawback for water borne coatings.

1.3 Glues

The loss of structural integrity due to the ingress of moisture into glued wood products. The moisture in the wood damages the wood glue interface and results in de-bonding and failure.

1.4 Objectives

This report seeks solutions to some specific problems through an improved understanding of the dynamics of water in wood. The principle objective is to understand better the behaviour of moisture in wood near the surface and at interfaces. This objective has two distinct areas within the project. The first is the improved understanding of the role and parameters of the surface layer (10-300 micrometers) during wood drying, which has the aim of reducing quality loss such as surface checking which is a problem in the wood industry and for end users. The second objective is an improved understanding of the moisture interaction at the interface between glue and wood, and coating and wood. Most moisture related problems with coated and glued wood starts at the interface.

2. Background

2.1 Garfield NMR

GARField, standing for Gradient At Right-angles to Field, is a small permanent magnet design that features shaped pole pieces that are optimised for profiling through thin, planar samples[1]. The magnet design was developed at the University of Surrey in response to a need for magnetic resonance (MR) profiling of planar samples and surfaces using stray field like methods. These methods exploit the very large magnetic field gradient surrounding a conventional high-field high-resolution super conducting magnet. The idea behind GARField was to develop a smaller permanent magnet of lower cost with a tailored and optimised gradient and magnetic field for profiling planar samples without many of the disadvantages of the high field system including non-optimum geometry and cost. In the conventional case, the static field and gradient are parallel whereas in GRAField they are orthogonal. GARField is ideally suited to high spatial resolution imaging of solid systems, confined liquids and in general samples exhibiting short NMR spin-spin relaxation times such as the wood surfaces, coatings and glues explored here.

The Mark I GARField magnet was available at the project outset[1], where it was dubbed an orthogonal gradient magnet to reflect this optimised geometry. During the project lifetime, and partly in response to the success of GARField in this and other projects, the UK EPSRC has funded a MARK II design and build with additional advantages[2]. The overwhelming majority of the work carried out in the MARWINGCA programme used the MARK I magnet with probes designed and built as part of the project.

---

[1] Glover P. M. et al., *J. Magn. Reson.*, 1999, 139, 90

[2] Bennett G. et al, to be published in Magn. Reson. Imag.

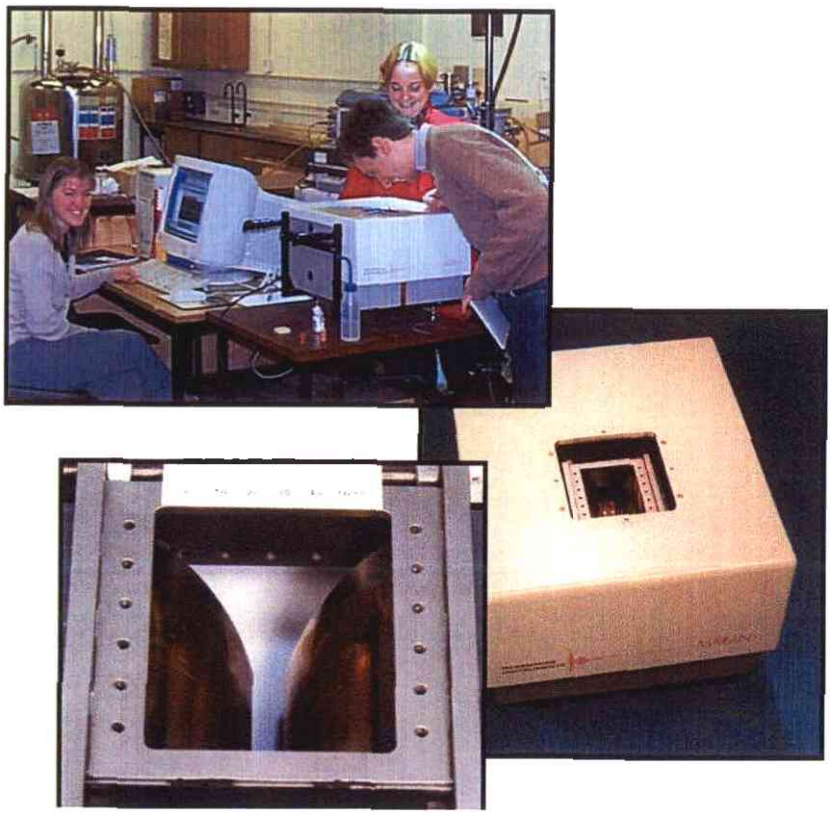

Figure 1. Views of the MARK I GARField used throughout this project, including the pole piece detail.

The GARField pole piece shaping is such as to yield a near horizontal (z-direction) magnetic field, B, of *constant magnitude* in the horizontal plane with a strong magnetic field gradient, G, in the vertical (y) direction as shown in figure 2 The required shape can be calculated analytically using a scalar potential method to solve the Laplace equation. The resultant field profile is characterised by a parameter equal to G/B. In the first implementation of the design, a belt-and-braces approach was adopted to ensure the realised magnetic field is as near specification as practically possible. The magnet is characterised by $G/B = 25$ m^{-1} and the minimum pole piece separation was fractionally over 10 mm. Access to the magnet pole pieces is only possible from above due to the symmetric design of the yoke and is thus severely restricted. Nonetheless, using this magnet and a small surface coil it has proved to be possible to profile ^{1}H through layers a few hundred microns thick with a pixel resolution of circa 7-15 μm and an echo time, 2τ, typically between 100 and 300 μs. With these parameters the principal limitations to resolution are the natural curvature or roughness of the sample and the extent to which the sample can be readily made level relative to the magnetic field.

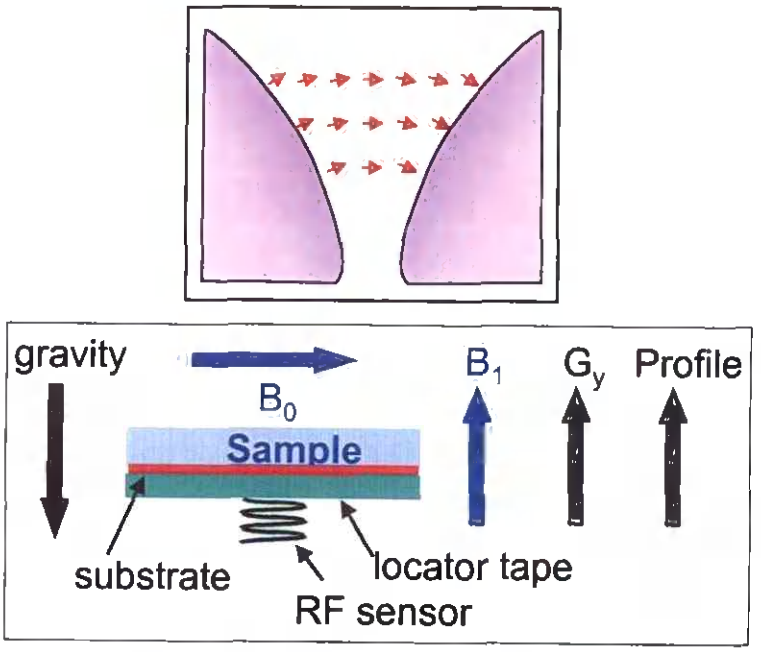

Figure 2. Schematic of the Garfield magnet pole pieces (top) and of the sample orientation geometry (bottom). The static field is B_0, the r.f. sensor field is B1 and the gradient is direction is G_y.

Several improvements to the design have been incorporated into the second GARField magnet which has recently been constructed. First, and most importantly, the yoke has been made into a C-frame and the frame has been rotated with respect to the poles so as to allow access both from above and from the sides. Side access dramatically improves the range of sample geometries that can be accommodated. Second, the magnet has been scaled by a factor of 3/2 so as to allow larger samples and probes to be used. Third, the pole pieces have been shaped both on their upper and lower sides *but with different curvatures*. This gives two values of *G/B* for the same pole piece pair, one characterising the space above the point of closest approach of the poles, $G/B = 16.67$ m^{-1} and the other the space below, $G/B = 33.33$ m^{-1}. This innovation permits analysis of samples at two contrasting gradient strengths but the same static field simply by raising or lowering the sample a few centimetres. The feature is expected to be of most use in determining the relative weighting of diffusion and spin relaxation in profile data. Finally, fixings for precise and reproducible mounting and alignment of sample probes have been designed in response to developments occuring in the MARWINGCA programme and incorporated into the magnet frame.

2.2 Wood surfaces

Wood drying is an important industrial process in the sawmill industry since it has a great impact on both the product quality and the manufacturing costs. Hence, several scientists have aimed to improve the industrial drying process by developing theoretical models of the drying

process:, Cloutier *et al.*[3] Perré[4]; Arfvidsson[5]; Hukka[6] and Salin[7] amongst others. These models need verification against experimental measurements. A weak point in some of the models is the description of the moisture transport above the fibre saturation point, FSP, and the behaviour at the surface interface. Usually the models use a moisture potential as the driving force for the moisture transport. Hence, there must be a gradient in the moisture content in the whole moisture content range otherwise the models will calculate zero flux. This drawback has been discussed by Wiberg[8] and Salin[9].

Recently, Wiberg[8] has studied drying in sapwood above FSP using a CT-scanner. He showed almost flat moisture profiles in the bulk at moisture contents above FSP. Furthermore, he showed what he called the formation of a dry shell that recedes as an evaporation front towards the bulk. Due to an edge effect in the CT-scanner Wiberg was not able to measure in the surface layer and the resolution, 240 µm, was not high enough. Tremblay[10] has also shown almost flat moisture profiles above FSP. He used a slicing technique with a resolution down to 380 µm.

The aim of wood drying experiments is to obtain measurements during drying of wood using MR in order to accurately describe the surface behaviour and then to compare this behaviour with theory.

2.3 Coatings

Coatings are used ubiquitously on wood for preservative and decorative purposes. For architectural finishes, oils and alkyds may be dissolved in a solvent and used in solvent borne coatings or emulsified in water and used in waterborne coatings. Acrylics are normally dispersed in water to be used in waterborne coatings. Tightening environmental legislation and improved performance / cost benefit are key drivers behind continued academic and industrially based research into the development of improved coating formulations. The objectives of the coatings work are to study with MR the moisture absorption / desorption behaviour of different types of coatings and in particular to study the impact of the presence of surface active substances such as surfactants on these coatings and their performance.

---

[3] Cloutier, A., Fortin, Y., Dhatt, G. 1992. A wood drying finite element model based on the water potential concept. Drying Technology 10(5): 1151–1181.

[4] Perré, P. 1996. The numerical modelling of physical and mechanical phenomena involved in wood drying: an excellent tool for assisting with the study of new processes. Proc. 5th International IUFRO Wood Drying Conference, 13-17 Aug., Quebec City, Canada.

[5] Arfvidsson, J. 1998. Moisture transport in porous media, modelling based on kirchhoff potentials. Doctoral thesis, Lund Institute of Technology , Sweden.

[6] Hukka, A. 1999. The effective diffusion coefficient and mass transfer coefficient of Nordic softwoods as calculated from direct drying experiments. Holzforschung 53, 534-540.

[7] Salin, J-G. 1999. Simulation models; From a scientific challenge to a kiln operator tool. Proc. 6th International IUFRO Wood Drying Conference, 25-28 Jan., Stellenbosch, South Africa.

[8] Wiberg, P. 2001. X-ray CT-scanning of wood during drying. Doctoral thesis, Luleå University of Technology, Sweden.

[9] Salin, J-G. 2002. Theoretical analysis of mass transfer from wooden surfaces. 13th International Drying Symposium, Aug. 27-30, Beijing, China.

[10] Tremblay, C. 1999. Détermination expérimentale des paramètres caractérisant les transferts de chaleur et de masse dans le bois lors du séchage. *In French*. Doctoral thesis, Université Laval, Québec.

The use of surfactants is essential for controlling the colloidal stability of the dispersion during synthesis, storage, application and film formation. Heilen *et al.*[11] review their different uses in waterborne coatings. Hellgren *et al.*[12] also review the use of surfactants in coatings. Pigments are dispersed by surface-active dispersion aids. Emulsions and dispersions are stabilised by surfactants, and foaming tendencies are depressed by surfactants. Anti-settling agents are also normally surfactants. Both dispersions and emulsions need surfactants to develop stable products. Typical concentrations of surfactants in waterborne coatings are in the range of 0.5 to 5 % (by weight) of the amount of resin. Even if the emulsion system is optimised with respect to emulsion stability, some 25 % of the non-ionic surfactant can be found in the continuous phase (*i.e.* water phase) due to the hydrophilic/hydrophobic character of the surfactants, Hofland and Schaap[13].

During film formation, phase separation occurs and the surfactants in the water phase may be mobilised and transported into the wood substrate. The surfactants can also be released by rain after film formation and either washed away or transported into the wood substrate. The chemical nature of surfactants, with a hydrophilic and a hydrophobic part in the molecule, causes them to accumulate at interfaces, where high concentrations may occur. Bradford and Vanderhoff[14] noticed the exudation of incompatible surfactants during ageing of latex films. They investigated nonyl phenol-ethylene oxide adducts of varying chain length. The long-chain, hydrophilic, compounds were found to exudate towards the film surface, whereas the short-chain, lipophilic surfactants remained in the film. The presence of surfactants in latex films has been shown to strongly influence the adhesion properties, Charmeau *et al*[15]. A literature survey on the role of emulsifiers in latex films has been carried out by Bindschaedler *et al*[16]. The water absorption properties of different types of rheology modifiers (*i.e.* thickeners) have been studied by Shay *et al*[17]. They found that there is a high degree of water vapour sorption differentiation between different types of thickeners. Their study was performed on pure substances and not in combination with any coating or substrate. Tzitzinou *et al.*[18] found that anionic surfactants are always present at the surface of the acrylic latex films, regardless of the film-forming conditions.

---

[11] Heilen, W., Klocker, O. and Adams, J. (1994) Influence of Defoamers on the Efficiency of Waterborne Coating System.," Journal of Coatings Technology, **66**, No. 829, 47-53.

[12] Hellgren, A-C (1998) Probing polymer interdiffusion in carboxylated latices with force modulation atomic force microscopy. Progress in Organic Coatings **34**, 91-99.

[13] Hofland, A. and Schaap, F. J. (1990) Alkyd Emulsions for High Gloss Paint Systems; Old Properties in New Particles. Färg och Lack Scandinavia, **9**, 182-192.

[14] Bradford, E. B. and Vanderhoff, J. W. (1972) Additional Studies of Morphological Changes in Latex Films, Journal of Macromolecular Science-Phys., B6(4), 671-694.

[15] Charmeau, J. Y., Kientz, E. and Holl, Y. (1996) Adhesion of latex films; influence of surfactants. Progress in Organic Coatings **27**, 87-93.

[16] Bindschaedler, C., Gurny, R. and Doelker, E. (1987) Influence of Emulsifiers on Film Formation from Cellulose Acetate Latexes, Experimental Study of Phase Separation Phenomena Due to Sodium Dodecyl Sulfate. I. Journal of Applied Polymer Science, Vol. **34**, 2631-2647.

[17] Shay, G. D., Olesen, K. R. and Stallings, J. L. (1996) Predicting the Water-Sensivity of Film-Forming Coatings Additives by Water Vapour Sorption: With Application to Thickeners and Reology Modifiers. Journal of Coatings Technology, **68**, No. 854, 51-63.

[18] Tzitzinou, A., Jenneson, P. M., Clough, A. S., Keddie, J. L., Lu, J. R., Zhdan, P., Treacher, K. E. and Satguru, R. (1999) Surfactant concentration and morphology at the surfaces of acrylic latex films. Progress in Organic Coatings **35**, 89-99.

Surfactant migration and enrichment at coating interfaces have been reported. Juhue *et al.*[19] have shown that addition of a coalescing aid to a latex dispersion greatly enhances surfactant migration. Torstensson *et al.*[20] found using ESCA spectra that a lacquer film containing 1% (by weight) of a monomeric surfactant my have an average surface surfactant concentration of around 50%. Zhao *et al.*[21] have shown that enrichment of sodium dodecyl sulphate (SDS) in acrylic latex films occurs at both interfaces (film/air and film/substrate) but that it is more pronounced at the film/air interface. Roulstone *et al.*[22] conclude that the type and concentration of surfactant used can significantly influence the water permeability of latex films. Higher concentration of surfactant results in higher permeability due to phase separation in the film. There are five possible regimes of deposition of the surfactant during film formation: (i) it dissolves and migrates into the polymer; (ii) it is excluded to the latex film surface; (iii) independent volumes rich in surfactants are formed which may or may not be located at the interstitial voids between the particles; (iv) a continuous network of surfactant is formed and (v) it remains adsorbed on the particle surface as a monolayer.

It has also been shown that an excess of surfactants in a coating has a negative effect on the ability of a coating to prevent water ingress, which most probably is due to the hydrophilic character of the surfactant, Ekstedt[23,24].

2.4 Glues

Gluing of wood is a critical step in the manufacture of wood products. Glue performance and durability have obvious implications for product lifetime and fitness-for-purpose. Gluing can be split into three phases: glue spread, assembly and pressing. Depending on product these phases take more or less time. Directly after the glue spread, loss of water from the glue line is started through evaporation to the air and diffusion into the wood substrate. After the assembly, the evacuation of water only occurs through diffusion into the wood substrates.

Knowing with high accuracy the rate of water evacuation through evaporation and absorption during the different process steps makes modelling of the hardening behaviour easier and generally provides a better understanding of the glue curing process.

The drivers to gaining an improved understanding and hence definition of glue hardening are the need to shorten the press time and to achieve maximum productivity without increasing the risk of delamination. For non-load-bearing constructions, delaminations lead to relatively

---

[19] Juhue, D., Wang, Y., Lang, J., Leung, O-M., Goh, M. C. and Winnik, M. A. (1995). Surfactant exudation in the presence of a coalescing aid in latex films studied by atomic force microscopy. Journal of Polymer Science Part B: Polymer Physics. **33**, 7, 1123-1133.

[20] Torstensson, M., Rånby, B. and Hult, A. (1990) Monomeric Surfactants for Surface Modification of Polymers. Macromolecules, **23**, 126-132.

[21] Zhao, C. L., Holl, Y., Pith, T. and Lambla, M. (1989) Surface Analysis and Adhesion Properties of Coalesced Latex Films. British Polymer Journal **21**, 155-160.

[22] Roulstone, B. J., Wilkinson, M. C. and Hearn, J. (1992) Studies on polymer latex films: II Effect of surfactants on the water vapour permeability of polymer latex films. J. Polymer International **27**, 43-50.

[23] Ekstedt, J. (1995) Moisture Dynamic Assessment of Coatings for Exterior Wood". Licentiate thesis. TRITA-BYMA 1995:12 Kungliga Tekniska Högskolan, Stockholm. ISBN 91-7170-728-X.

[24] Ekstedt, J. (2003) Influence of Coating System Composition on Moisture Dynamic Performance of Coated Wood, Journal of Coatings Technology, **75**, No. 938, 27-37 (2003)

costly customer complaints. For load-bearing constructions, delaminations might be hazardous.

The objective of the work reported here is to show in a systematic study how MR can be used to characterise the glue hardening process. Parameters like glue storage temperature, hardener type, hardener content, glue line thickness and hardening temperature are varied in order to measure their impact on hardening time.

When there are differing climate conditions on either side of a laminated wood product, a moisture flow is developed through the product due to diffusion. The glue line might then be an obstacle to this moisture flow. In some cases this might be positive when a moisture diffusion barrier is wanted. However, if the glue line acts as a diffusion barrier and the water cannot escape from whence it came, then there is a subsequent risk of glue line delamination and after longer exposures to high moisture content, wood rot.

As a second objective, liquid moisture diffusion in laminated wood has been studied in order to achieve a better understanding of how to design future glued products with higher durability in service life.

3. Instrumentation Development

The project called for the optimisation of the GARField MR measurment process for the specific systems studies and for the design and manufacture of a range of appropriate MR probes and samples mounts.

3.1 Probes

3.1.1 Drying probe

A probe was constructed to allow visualisation of surfaces subjected to a controlled humidity, temperature and air flow conditions. Additionally, an environmental control unit was constructed. The probe is shown in figure 3a and b.

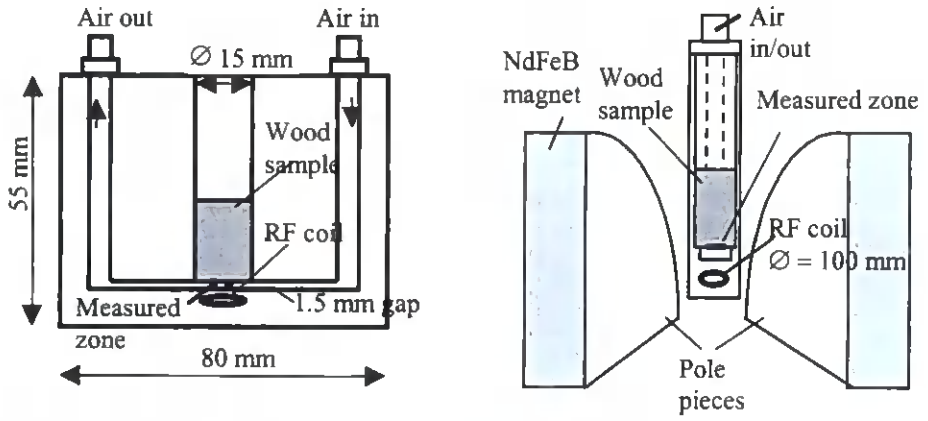

Figure 3a (left) and b (right). (a) Sample holder and RF probe, seen from the long side. (b) Sample holder and RF probe, located between the curved permanent magnet pole-pieces.

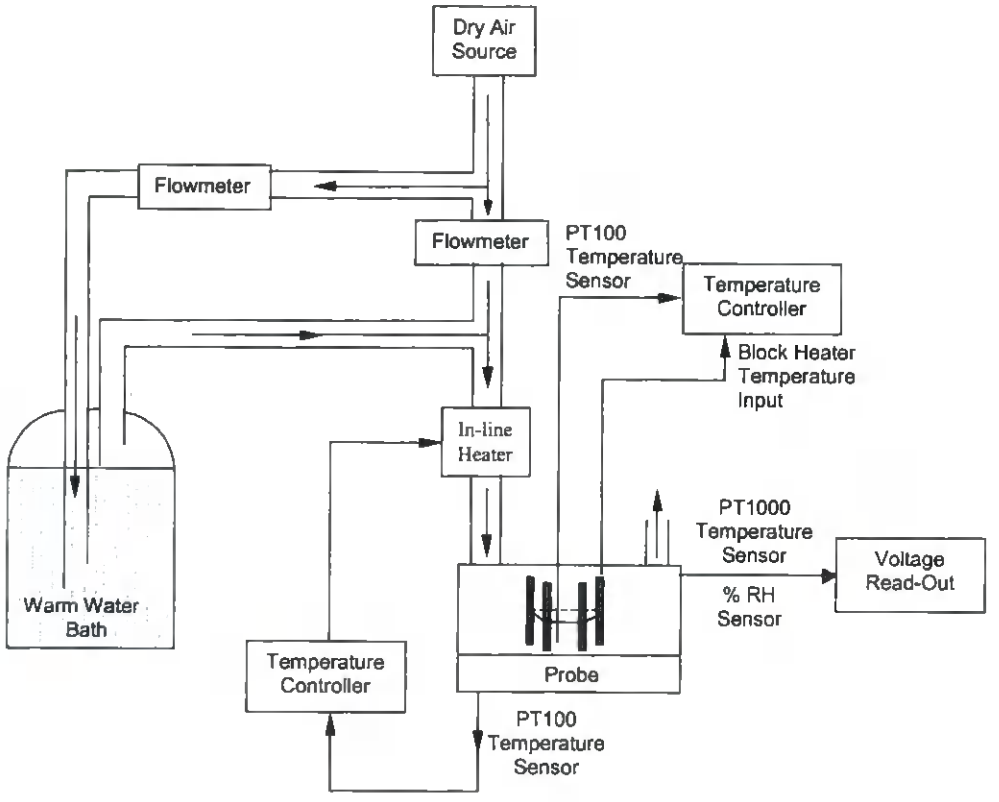

Figure 4. Schematic of the air-control system.

The probe consists of a sample holder made primarily of PTFE with a built-in radio-frequency (r.f.) coil. PTFE is hydrogen free and therefore invisible to MR. The sample is placed in the central cavity of the probe with the surface to be examined lowermost. The sample rests on a small lip above a channel 1.5 mm deep through which temperature and humidity controlled air passes. The air thus flows over the exposed sample surface. The air enters from the hole / connector at one end of the probe and exits the other. The sample is weighted down within the cavity to prevent it lifting when the air flows and the central cavity is stoppered. The RF coil is embedded in the base of the probe, which, since it is below the sensitive volume is made of Perspex. The diameter of the RF coil is 10 mm and it is tuned to 30 MHz using high voltage ceramic chip capacitors. The probe assembly fits between the magnet pole-pieces so that the

critical surface of the wood sample inside the probe is situated at the correct magnetic field during the experiment. Non-inductively wound heating coils, two PT100 resistance thermometers and resistive humidity sensors are built into the probe with the humidity sensor in particular placed in the air flow. Two thermometers are used: one near the heaters to control the temperature of the probe body, the other close to the sample surface to measure the air temperature.

The air temperature and humidity control is shown schematically in figure 4. Dry air is fed to the unit. Part of the air is bubbled through a warm water bath and attains high humidity at elevated temperature. The remaining dry air is heated but not wetted. The two air streams are subsequently mixed to yield air of controlled elevated temperature and humidity. The relative air flows in the two paths are controlled by electronically operated needle valves.

The greatest difficulty in using this system is to prevent condensation of water in the MR probe at high humidities. It is also difficult to achieve high temperatures for the air due to the considerable thermal mass of the probe and heat leaks to ambient. Nonetheless, it was possible to study interfaces up to 50° C at humidities of the order of 80% with the system although, in practice, most work has been carried out at room temperature where temperature stability and hence data quality was much improved.

3.1.2 Coatings probe

A second probe was constructed to study coatings. Coatings potentially require a greater field of view than is readily obtainable using a fixed frequency coil in the permanent field gradient where the field of view is limited by the transmitter and receiver bandwidths rather than the depth of penetration of the RF irradiation into the sample. This latter depth is of the order of the coil radius, a few millimetres. The solution investigated was to build a probe with an electronically tuned coil using voltage controlled tuning diodes in the tuning elements of the receive coil and a second, fixed broad band transmit coil. The coil can be re-tuned under computer control synchronously with changes in the transmitter frequency so as to optimise the coil to interrogate at different levels throughout the sample.

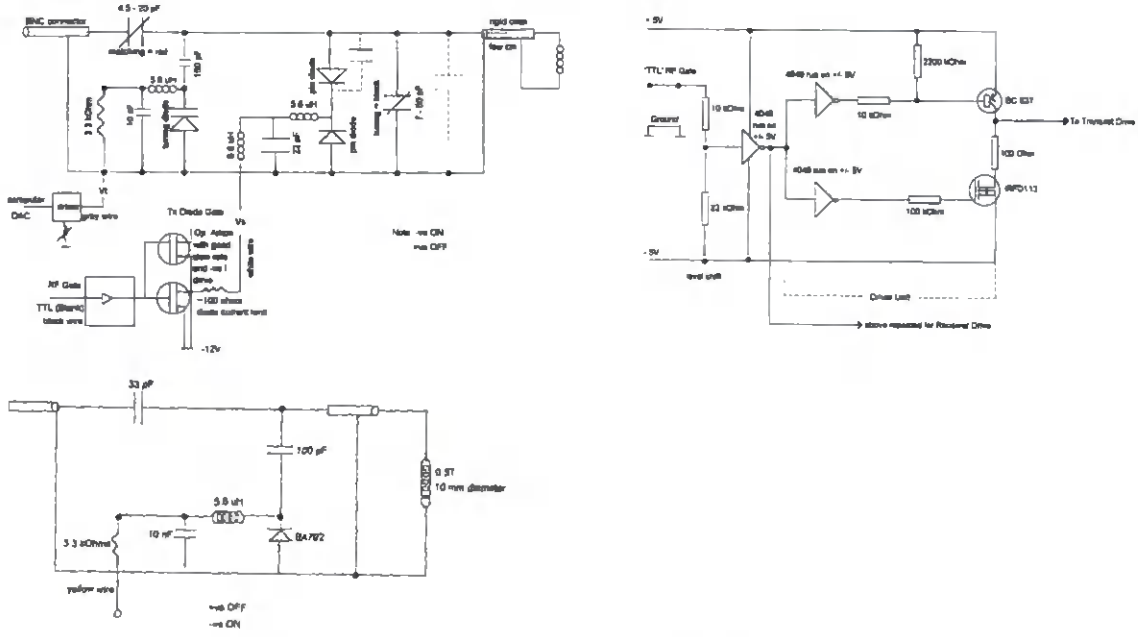

Figure 5. Schematics for the coatings probe transmit, receive and control circuits.

The first constructed version of the probe had switched coils for RF transmission and reception as shown in figure 5. This was because it was felt that the voltage controlled devices would not tolerate the high transmission power of the RF. In practice the switching circuit proved too slow to use routinely for MR and the switching circuit introduced considerable electrical noise. It was found that the voltage controlled diodes could withstand the high voltages of the transmit circuit for the short duration RF pulses without serious degradation. Consequently, this first version was eventually abandoned in favour of a second version of the circuit which used a single electronically tuned transmit / receive coil based on the receive coil without switching (permanently on) already shown. It worked adequately. The greatest difficulties in using the coil were (i) the computer interface due to the specific structure of the version of Resonance Instruments Maran software available to the project and (ii) the need to recalibrate the pulse length at different frequencies appropriate to different depths into the sample and the consequent effect this had on the excited slice width. In use, the experiment design was a compromise between having many slices each of narrow bandwidth so as to improve the signal to noise ratio of each measurement and few slices of greater bandwidth. In each case the slices needed to be interwoven using software to form a single profile. The time required to change and stabilise the coil between frequencies and need for calibration were major factors in the decision. Ultimately, the data obtained was not of significantly better quality than using a simple single coil and both tuneable and fixed coils were used in data acquisition.

Figure 6. The final coatings probe (shown without the sample mount). The probe was designed to profile down into a sample without touching the sample. The tuning circuitry is built into the handle.

3.1.3 High Pressure Probe

An attempt was also made – additional to the original project objectives – to build a high pressure probe for GARfield, figure 7. A probe was constructed as shown in . However, it was not used routinely because of its considerable weight (due to the apparatus required to generate the pressure) and the difficulty of keeping the sample aligned as pressure was applied.

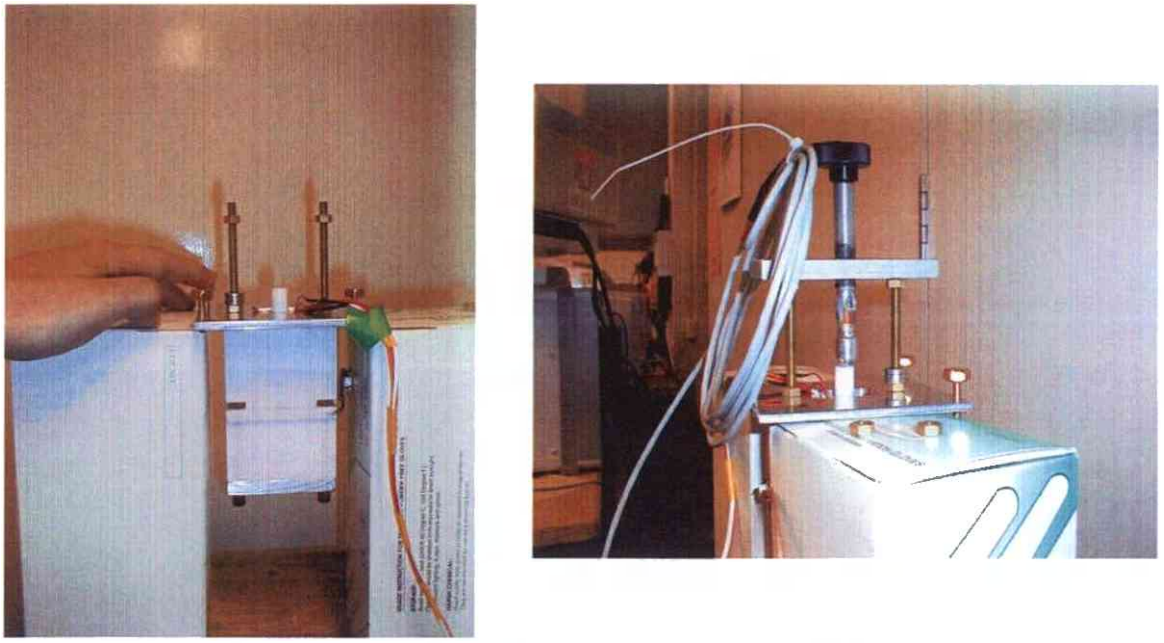

Figure 7. The high pressure probe before mounting into the magnet. Pressure is applied via the top screw (right) and measured using strain gauges.

3.1.4 Probe levelling

A major issue for GARField MR profiling is sample levelling. The surface to be inspected must be orthogonal to the (invisible) magnetic field gradient to a high degree of accuracy. A standard three-contact-point kinematically-designed mounting plate was introduced onto which all the probes could be mounted. Use of probes mounted on these plates greatly improved the ease of sample levelling and improved both data quality and throughput as a result. Probes could be removed from and replaced within the magnet to a high degree of accuracy allowing easier sample change.

3.1.5 Pulse sequences and pulse sequence parameters

A key objective of the project was to optimise RF pulse sequences for use with GARField. In order to insure high throuput of samples, it was necessary to be confident that pulse sequences chosen were robust and as near optimal as possible for the sample type (wood surface, coating layer, glue line) under investigation. The multiple quadrature echo sequence is the workhorse of GARField[25]. The sequence is defined as $90_x\text{-}\tau\,(90_y\text{-}\tau\text{-echo-}\tau)_n$ where $90_{x/y}$ is a pulse of nominal flip angle 90° or $\pi/2$ and relative phase x or y. τ is a short interval – the pulse gap. n is the number of echoes, figure 8. The sequence is repeated at intervals of the so-called

[25] McDonald P. J., Newling B. *Rep. Prog. Phys.* **61** (1998) 1441

repetition delay, R_D. The pulse flip angle varies dramatically across the sample but is typically $\pi/2$ at the centre of the interrogated region. This corresponds to a pulse length of 1.5 μs using a 300 W amplifier and a small 4 turn coil of about 3 mm diameter. The maximum (one sided) field of view is then circa 1.5 mm. The pulse gap is kept sufficiently short that the first echo observed is not seriously affected by T_2 decay and therefore is a measure of proton density.

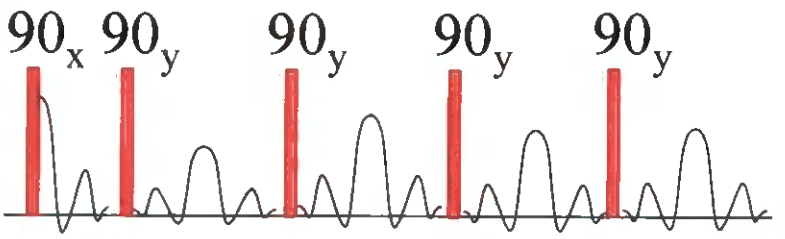

Figure 8. The standard multiple quadrature echo pulse sequence used throughout.

Complete, typical parameter sets as used for many of the experiments are given in Appendices A, B and C for wood surface drying, coatings, and glue layers respectively.

The data analysis was usually to Fourier transform each separate echo and then to co-add the echoes to improve the signal to noise ratio of the profile. When further discrimination and contrast was required, for instance between mobile and less mobile protons, then the echoes were co-added in blocks of four or eight so as to yield profiles variously weighted to different relaxation times. Careful choice of τ and R_D enabled profiles of different molecular mobility weighting to be generated.

It should be noted that, unlike normal MRI, the strong steady gradient causes rapid signal decay of mobile species due to diffusion. These do not therefore show as the longest lived components in the signal. This causes some complication in data interpretation.

4. Experimental

4.1 Wood surface drying measurements

High resolution moisture content profiles have been measured during drying in surface layer (0 – 300 μm) of wood. Results have been published in the open literature[26,27]. For comparison measurements have also been performed with samples of concrete. The majority of the experiments were performed on samples of Scots pine (*Pinus sylvestris*) sapwood and heartwood which originated from Dala-Järna in Sweden. Further experiments were performed on samples of Norwegian spruce. The samples were shaped as small round cylinders with a diameter of 14 mm and a length of 20 mm. During the experiments the temperature varied from room temperature up to 46 °C and the relative humidity was varied between 16% and 100%. In the experiments reported here, the air velocity used was 1.9 m/s. This air velocity yields a drying capacity comparable to that in an industrial kiln, see section 4.2.

---

[26] Rosenkilde, A. and P. Glover. 2002. High Resolution Measurement of the Surface Layer Moisture Content during Drying of Wood Using a Novel Magnetic Resonance Imaging Technique. Holzforschung **56**, 312-317.

[27] Rosenkilde A. GorceJ.-P. and Barry A. accepted for publication in Holzforschung.

The GARField magnet was used at a field strength at the sample surface of nominally 0.7 T (see section 2.1) together with the specially built drying probe (see section 3.1.1). The strong field gradient of approximately 17 Tm^{-1} directed into the sample surface gives a very high profile spatial resolution in this direction. A slight downward force was applied to the sample to ensure that the surface did not move during drying. Between the wood surface and the RF coil there was a 1.5 mm gap where a climate controlled airflow transported away the water that evaporates from the wood surface. The achieved spatial resolution in the experiments varied according to the precise experimental parameters chosen between 13 and 21 μm with a field of view of 300 and 600 μm. Experimental parameters are given in Appendix A: Optimised parameters for GARField drying experiments.

4.2 Air velocity calculation

It is necessary to ensure that the wood drying capacity of the experiments corresponds as closely as possible to that of an industrial kiln. In the experiments performed the air velocities used are typically 1.9 m/s. This air velocity is to be compared to an air velocity of approximately 2 - 5 m/s in an industrial kiln. Equally, the air flow channel gap in the experiments is 1.5 mm whereas it is typically 25 mm in the industrial kiln. Comparable air velocities correspond to equal heat transfer coefficients for both 1.5 and 25 mm air gaps. For the air flow, the Nusselt number is defined by

$$\mathrm{Nu} = \frac{\alpha d}{\lambda}$$

and the Reynolds number by

$$\mathrm{Re} = \frac{vd}{\nu}$$

where α is the heat transfer coefficient (W/m^2K), d is the air gap (m), λ is the heat conductivity of air (W/mK), v is the air velocity in the air gap (m/s) and ν is the kinematical viscosity (m^2/s). It has been shown experimentally[28] that

$$\mathrm{Nu} \propto \mathrm{Re}^{2/3}$$

Consequently, for equal heat transfers, the experimental conditions correspond to a kiln air velocity of approximately 3.9 m/s, within the range of an industrial kiln.

4.3 Coatings measurements

Three different commercial coating systems have been studied in the project. The three systems were one alkyd emulsion paint, one all acrylic paint and one two-pack polyurethane industrial paint. In addition to these systems, the reference coating system "Internal Comparison Product" (ICP), as specified in European standard EN 927 - 3, has been studied. The composition of this ICP is given in the standard. The ICP is a normal solvent-borne alkyd paint.

[28] Söderström,O. 1987. Computer simulations of a progressive kiln with longitudinal air circulation. Forest Products Journal 37:25-30.

The different coatings have been tested for water absorption value according to EN 927 - 5. The water absorption value is a measure of the water protecting performance on wood. The values for the different coating systems are shown in Table 1. The water absorption value shows the amount of water that passes through a coating on wood during a wetting period of 72 hr.

Table 1. Water absorption values for the coatings used.

Coating system and identifier	**Water absorption value (g/m^2)**
Acrylic paint (samples "F")	175
Alkyd emulsion paint (samples "S")	250
Internal Comparison Product (samples "ICP")	110
Polyurethane (samples "PU")	140

MRI operating conditions for the different samples and measurements were normally kept constant although certain parameters in some measurements had to be slightly modified in order to get stable and reliable measurements. For samples F2, (i.e. acrylic paint, 2nd variant sample) F3, S1, S2, ICP and PU the nominal gradient strength of 17 T/m was used and the calculated pixel resolution was 14 μm, with a field of view (window) of about 1.6 mm. The pulse length was kept deliberately short to excite a large detection bandwidth. The peak from the marker reference tape on the coil was set close to the left of the field of view, and the dwell time was reduced to give a useful image window within the field of view of around 1.4 mm. The minimum τ, which could be used with these settings, was 70 μs. All sample profiles shown are normalised with reference to an elastomer standard to correct for the fall off in detector sensitivity with distance from the coil. The elastomer standard is assumed to have uniform proton density and relaxation.

The coating probe had automatic frequency switching. This enabled slices at different depths in the sample to be measured. Normally it was used with 30 linear steps of 70 kHz covering a total of around 2 mm. An echo train is collected (α_x-τ-(2α_y-τ-echo-τ)$_n$) at each frequency step. The intensity of the echo train is used to give the intensity of a single point at that frequency. The frequency relates to a set position in the sample. The excitation bandwidth, filter width and detection bandwidth is kept deliberately narrow so that the slices do not overlap. The data is subject to a fall off in intensity with distance from the coil. To correct for this all data is normalised with an elastomer standard, which should result in a rectangular profile for uniform proton density and relaxation.

4.3.1 Samples F2, F3, S1 and S2

Test samples labelled F2, F3, S1 and S2 were pieces of machined pine wood 12 mm in diameter, 7 mm long. They had the sides coated with polyurethane varnish, one face left open and to the other face was applied the coating sample (either 'F' or 'S'). The samples were placed into a PTFE cell, which was designed to hold a water reservoir 10 mm in diameter, 1 mm thick directly in contact with the coating. This cell was then placed into the coatings probe with the water adjacent to the probe, the water in contact with the coating, and the open face of the sample away from it.

For the water ingress experiments samples were placed on a wet sponge outside the instrument with the coating facing the sponge. At the measurement time the samples were quickly dried on a paper towel and weighed. Profiles were taken with the sample sandwiched between two glass cover slips to prevent it from drying during the measurement time. A redistribution of water is evident during the sampling time for some of the samples (see results section). Measurements were made for 120 hours. The samples were then turned over and stood on a glass surface in a desicator over silica gel and further profiles taken for 48 hours when the samples were found to have returned to their starting weight. Profiles were measured of both ends of the sample.

Profiles of the samples were measured using the thin film coil using the standard pulse sequence (α_x-τ(α_y-τ-echo-τ)$_n$) with the settings given in Appendix B: Optimised parameters for GARField coatings experiments.

4.3.2 Samples ICP and PU

Test samples labelled ICP and PU were 12 mm in diameter, 6 mm long. They had the sides coated with polyurethane varnish, one face left open and to the other face was applied the coating sample (either 'ICP' or 'PU'). The samples had been stored prior to analysis in a dark cupboard at 21°C and approximately 50% RH.

For the water ingress experiments samples were placed on a wet sponge outside the instrument with the coating facing the sponge. At the measurement time the samples were dabbed dry on a paper towel and weighed. Profiles were taken with the sample sandwiched between two glass cover slips to prevent it from drying during the measurement time. Measurements were made for 120 hours. The samples were then turned over and stood on a glass surface in a desicator over silica gel and further profiles taken for 48 hours when the samples were found to have returned to or lower than their starting weight. Profiles were measured of both ends of the sample.

Profiles of the samples were measured using the thin film coil using the standard pulse sequence (α_x-τ(α_y-τ-echo-τ)$_n$) with the settings given in Appendix B: Optimised parameters for GARField coatings experiments.

4.4 Glue measurements

The individual processes of evaporation and diffusion during an "open condition" of a glue can be separated with Garfield using a combination of wood / glue / glass sandwiches as shown in figure 9. The velocity of evaporation alone can be quantified by measuring the change of a test piece thickness with time for glue on top of a glass cover slip (figure 9b). The velocity of diffusion into the wood alone can be quantified by measuring the change of glue line thickness with time for glue between a wood substrate and a glass cover slip (figure 9c). The two effects should be more or less additive.

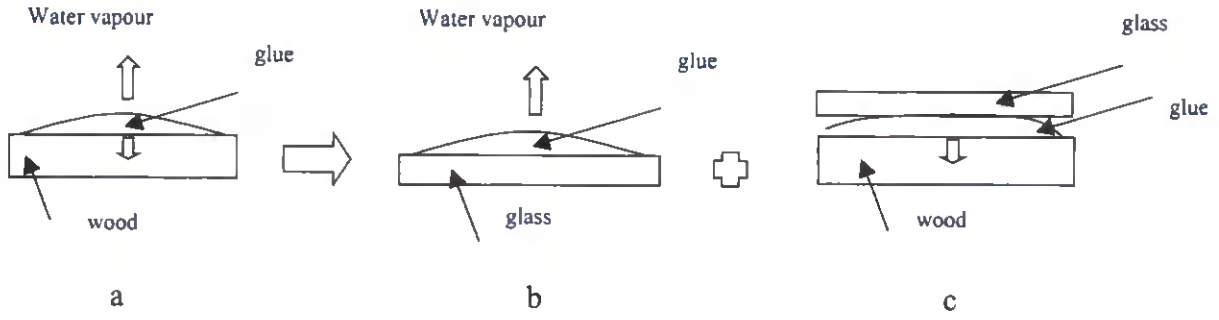

Figure 9 a). Glue spread on a wood substrate with evaporation of water to the air and absorption of water into the wood. b). Glue spread on a glass substrate with evaporation of water to the air. c). Glue spread on a wood substrate with absorption of water into the wood. The glass on top of the glue will prevent evaporation and make the determination of the position of the interface more accurate.

When applying the second substrate to the assembly, the "closed condition", the production process is reached. Provided the glue line is sufficiently thick, this situation should correspond to twice the absorption rate measured in the experiment shown in figure 9c or figure 10b.

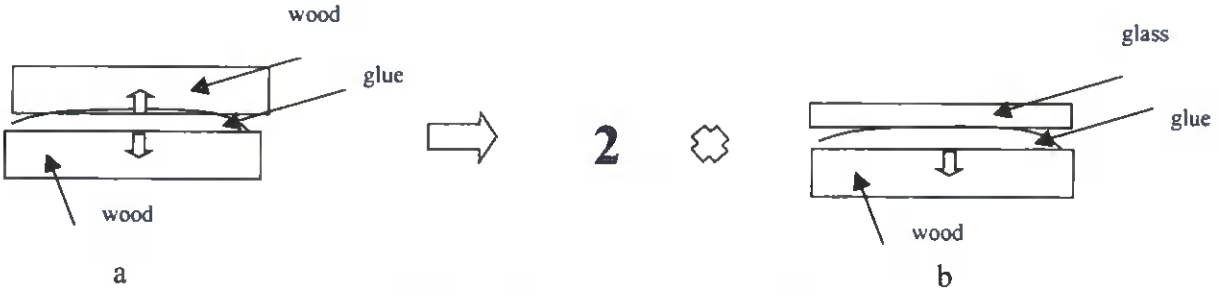

Figure 10 a). Glue between two wood substrates. b). Glue spread on a wood substrate with absorption of water into the wood. The glass on top of the glue will prevent evaporation and make the determination of the position of the interface more accurate.

Through out the work, 0.1 mm thick glass cover slips and for the most part 0.5 mm thick, pine veneer were used as substrates in different configurations although Spruce was used in some studies. An elastomer marker was put on top when appropriate to facilitate an identification of a sharp interface. Three wood glues were used: polyvinyl acetate, (PVAc); urea formaldehyde, (UF) and phenolic resorcinol formaldehyde (PRF) resins. The glues and hardeners were manufactured by Casco Products, Sweden. All three are available in liquid form. PVAc glue consists of the polymer dispersed in water. It forms a glass on drying. UF and PRF are two-component, "glue" and "hardener", systems. They cure at room temperature forming highly crosslinked networks. In particular, the UF consists of Cascorit 1205 together with one of the three hardeners: 2580 (ammonium chloride), 2508 (ammonium salt) or 2553 (aluminium sulphate). According to the manufacturer, hardener 2508 cures most quickly with a working time of 15 minutes at 20°C; 2553 has a working time of 1 hour and 2580 has a working time of 2 hours. The glue was mixed in the ratio100 parts glue to 20 (±2) parts hardener. Wood samples prepared from Scot's pine and spruce were sliced in the radial

direction to 0.5 mm thick and cut to 18 mm × 18 mm. Prior to use the wood was stored at 21°C and at approximately 50% relative humidity for several weeks.

For curing studies, the glue was spread onto one piece of wood and contacted either with a glass slide or second piece of wood. This second layer had an elastomer marker on the opposite face. The marker was used to estimate changes in sample thickness and was . The samples were first stood for 5 minutes after which they were lightly pressed together to alleviate the effects of initial wood warping. The samples were then transferred to the GARField sample stage for temporal and spatial measurements of curing typically over 2 hours.

For water penetration studies, the UF, PVAc and PRF glued layers were prepared using two 0.5 mm thick pine layers and were cured in a press at 70°C and 0.5 MPa. A PTFE cylinder was cemented to the top wood surface to contain a reservoir of water. Measurements started immediately after the water was added and continued for 24 hours.

The measurements were performed at a position where the magnetic field strength is 0.7 T and the gradient strength 17.5 T/m. A planar surface coil is used. A Mylar film is positioned above the coil to provide a position and intensity reference. The sample is placed on top of this, usually mounted on a glass cover slip. As with the wood drying and coating measurements, a quadrature spin-echo Fourier transform methods was used with an echo train: α_x-τ-(α_y-τ-echo-τ)$_n$ to collect the data. For the glue measurements, the number of echoes, n, is typically 16, the pulse gap, τ, is 70 μs the dwell time is 0.7 μs and number of points per echo is 128 yielding a pixel resolution and field of view of 15 and 1900 μm, respectively. However, only about 1600 μm of the available field of view yielded data with a useful signal-to-noise ratio due to the limited range of sensitivity of the surface coil. The number of co-added scans for signal averaging is typically 512 with a repetition time of 1.0 seconds, giving rise to a temporal resolution of 8.5 minutes, Appendix C: Optimised parameters for GARField glue line experiments. The profiles shown are the sum of the Fourier transforms of all echoes collected.

5. Results and Discussion

5.1 GARField profiling of wood surface drying

5.1.1 Pine

The analysed results from some of the experiments on Scots pine sapwood and heartwood are presented in figure 11, figure 13 and figure 14.

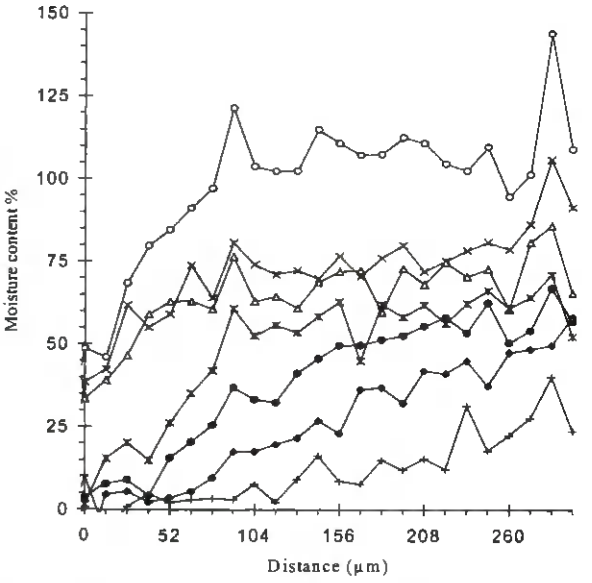

Figure 11. Moisture content profiles for Scots pine sapwood dried at 43 °C to 46 °C with a relative humidity of 16% to 18%, circles 0.5 h, crosses 1 h, open triangles 2 h, asterix 4 h, closed circle 7 h, diamond 19 h, plus 24 h.

The surface interface of the sample is assumed to be at 0 µm on the distance axis in these figures 11, 13 and 14. Due to resolution broadening the sample interface was not exactly at 0 µm. The sample interface was in the measurements more like a thin zone due to three factors, the first being sample alignment. The sample was never exactly aligned with the magnetic field. This gives a measured zone that contains both of sample material and air. The proportion of air in that zone increases with distance from the bulk. This affects the signal profile in a way that it will decay as the proportion of material decreases. The second factor is the roughness of the surface that will have the same effect on the measured profile as the sample alignment. The roughness of the surface is of the same magnitude as the diameter of a wood cell, figure 12. The third factor is the shift between the sample surface and the end of the last pixel. The pixel size is 13 or 21 µm. This factor will also affect the signal profile since the sample surface will not end exactly where the pixel ends. Therefore, the last pixel containing signal from the sample material will contain both sample material and air which will lower the measured signal in the last pixel, resulting in an observed decay in the measured profile.

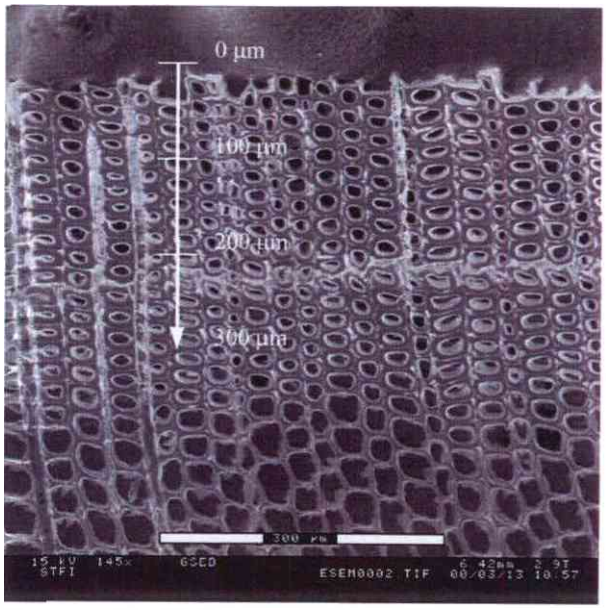

Figure 12. ESEM image of a part of the measured zone in the Scots pine sapwood sample. The image shows the wood structure across the grain and the axis shows the field of view in the measurement, magnification 145x. In this image it can be observed that the measurements have been made in the late wood.

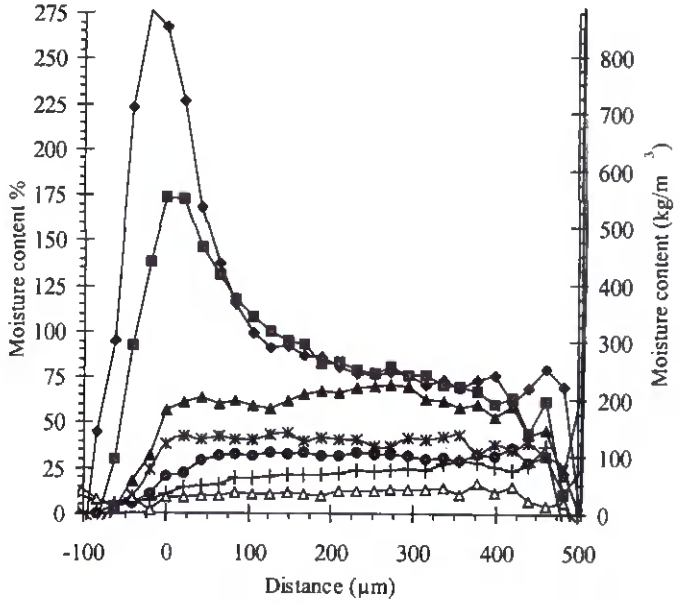

Figure 13. Moisture content profiles in Scots pine heartwood during drying 22° C. The actual surface is at 0 µm on the distance axis, diamond 0 min, closed square 5 min, closed triangle 9 min, asterix 16 min, closed circle 41 min, plus 56 min, open triangle 1254 min.

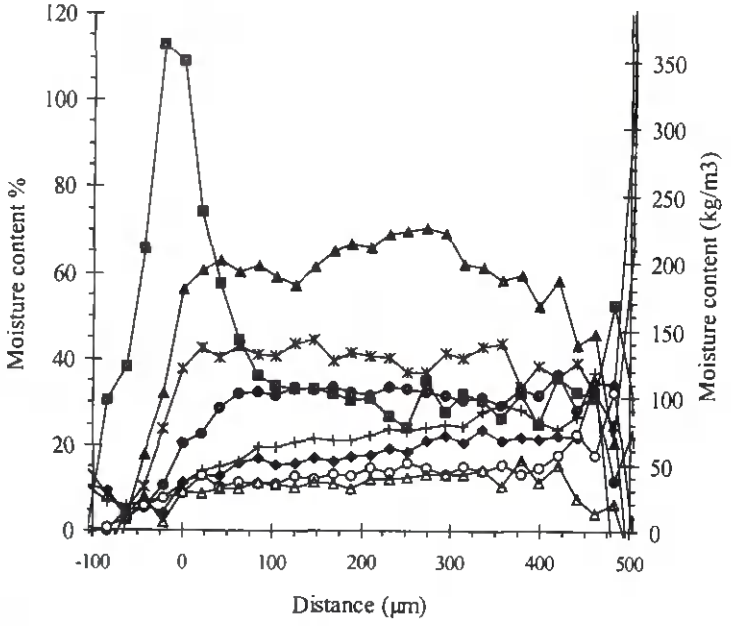

Figure 14. Moisture content profiles in Scots pine heartwood during drying and conditioning, enlarged version of figure 17 with a more narrow moisture content range. The actual surface is at 0 µm on the distance axis, closed triangle 9 min, asterix 16 min, closed circle 41 min, plus 56 min, open diamond 71 min, open circle 223 min, open triangle 1254 min, open square 1347 min.

5.1.1.1 Pine Sapwood

The sapwood result presented is from a measurement at 45 °C and a relative humidity of 17%. From the moisture content profile in figure 11, it can be observed that the profiles from 0.5 h to 4 h are almost flat without a gradient from a depth of 90 µm and further in. Furthermore, a steep gradient can be observed in those profiles from the surface to the depth of 90 µm. This indicates that the sample has dried a little during preparation of the experiment. Wiberg (1998) and Tremblay (1999) have also reported steep gradients near the surface at moisture contents above FSP. Their "dry shell" with the steep gradient was about 2 to 3 mm from the surface compared to 0.1 mm in this study. An explanation of that could be the difference in roughness of the wood surface. Wiberg (1998) and Tremblay (1999) used samples with sawn surfaces obtained from industrial production, whereas for this study, the surfaces were first sawn and then cut with a microtome resulting in a flat smooth surface.

The shape of the actual sample surface can be seen in figure 12, which is an Environmental Scanning Electron Microscope, ESEM, image. In the image, the roughness is about the size of a cell or less. The size of the cells is around 25 µm. This should be compared with a sawn surface where the roughness probably is around 0.5 - 1 mm. A more likely explanation of the difference between the present results and others is that it is a matter of resolution and field of view.

In figure 12 it can be observed that the measured zone consisted of only late wood, which has a higher density and lower diffusion coefficient than the early wood. The field of view of the MRI measurement is marked in figure 12 with an axis.

The accuracy in the moisture content profiles for sapwood is dependent upon the method for calibration and normalisation of the measured signal to moisture content. Since the NMR signal decreases with distance from the surface and the transmitting coil, each profile has to be normalised using a known profile. In these experiments a rubber phantom was used for normalisation profile.

Figure 11 shows a dramatic change in the moisture content gradient between 2 and 4 hours. A similar observation to this has also been made by Cloutier *et al.*[29] and Wiberg[30,31,32]. This is partly explained by Spolek and Plumb[33]. They state that there is a certain saturation where the liquid phase continuity is disrupted and liquid flow caused by capillary pressure is no longer possible as a moisture transport process. This is called the irreducible saturation. Below the irreducible saturation the moisture transport is mainly a diffusion process, which can be described by Fick´s law, viz.

$$g = -D\frac{\partial u}{\partial x}\cdot\rho$$

where g is the moisture flux (kg/m^{2}s), u is the moisture content (kg/kg), x is distance (m) and ρ is the wood density (kg/m^3). According to Fick's law the moisture flux g increases with an increasing gradient in moisture content, $\partial u/\partial x$. An increased gradient gives an increased inclination in the moisture content profiles. Further, if the gradient $\partial u/\partial x$ is equal to zero the moisture content profiles are flat and horizontal. At high moisture contents the moisture profiles are more or less flat and horizontal. According to Fick's Law the moisture flux g should be nearly zero, but quite opposite it is very high. An explanation to this behaviour is given by Wiberg[31] that concludes that the free water in sapwood migrates due to capillary forces towards the surface where bound water diffusion controls the drying rate.

5.1.1.2 Pine Heartwood

The heartwood results presented here is from measurements at 22 °C and a relative humidity of 55%. In figure 13 it is clearly seen that a lot of water ingress has taken place during storage in the sealed partly water filled plastic bags before the measurement started. The high amount of water close to the surface evaporates very quickly, after 9 minutes of drying the moisture profile is almost flat. The moisture profiles stay almost flat down to a moisture content slightly above 30% at 41 minutes of drying where a gradient starts to develop at the surface, figure 14. The profiles recorded after 41 minutes show all a gradient from the surface interface towards the bulk. This behaviour with almost flat profiles above a moisture content of approximately 30% and a gradient developing from the surface at lower moisture contents

---

[29] Cloutier, A., Fortin, Y., Dhatt, G. 1992. A wood drying finite element model based on the water potential concept. Drying Technology 10(5): 1151–1181.

[30] Wiberg, P. 2001. X-ray CT-scanning of wood during drying. Doctoral thesis, Luleå University of Technology, Sweden.

[31] Wiberg, P. 1995. Moisture distribution changes during drying. Holz als Roh und Werkstoff 53: 402

[32] Wiberg, P. 1998. CT-scanning of moisture distributions and shell formation during wood drying. Licentiate thesis, Luleå University of Technology.

[33] Spolek, G.A., Plumb, O.A. 1981. Capillary pressure in softwoods. Wood Dci. Technol. 15: 189-199

has been reported before, Rosenkilde and Arfvidsson[34], Tremblay *et al.*[35], Wiberg[30], Rosenkilde and Glover[36] and Salin[37].

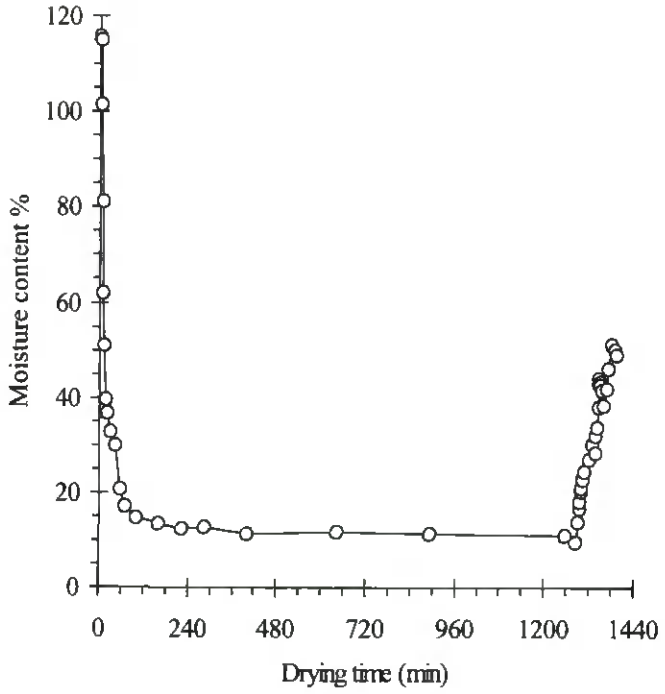

Figure 15. Mean moisture content in the surface layer, 0-300 µm, versus time for Scots pine heartwood dried at 22° C and RH of 55%.

The development of the mean moisture content in the measured zone can be observed in figure 15. It is clearly seen that the moisture in the surface layer (0-300 µm) evaporates very quickly and then sets at a nearly constant moisture content level. At the end of the drying period the climate is changed to wetter conditions and the moisture content is increasing a lot. At the end of the experiment, the relative humidity is 100% and therefore water condensation occurs at the sample surface. This can be seen in the moisture profile recorded at 1347 minutes in figure 14. A steep gradient with moisture content clearly above the fibre saturation point is detected at the surface interface. Without condensation at the surface interface, the moisture content never exceeds the fibre saturation point. During the whole drying period the

---

[34] Rosenkilde, A. and J. Arfvidsson. 1997. Measurement and evaluation of moisture transport coefficients during drying of wood. Holzforschung 51, 372-380.

[35] Tremblay, C., A. Cloutier and Y. Fortin. 2000. Experimental determination of the convective heat and mass transfer coefficients for wood drying. Wood Sci. Technol. 34:253-276.

[36] Rosenkilde, A. and P. Glover. 2002. High Resolution Measurement of the Surface Layer Moisture content during Drying of Wood Using a Novel Magnetic Resonance Imaging Technique. Holzforschung 56, 312-317.

[37] Salin, J-G. 2002. Theoretical analysis of mass transfer from wooden surfaces. 13th International Drying Symposium, Aug. 27-30, Beijing, China.

moisture content in the bulk changes from 70.5% to 53.4% which implies that there is a moisture flow going through the relative dry wood surface.

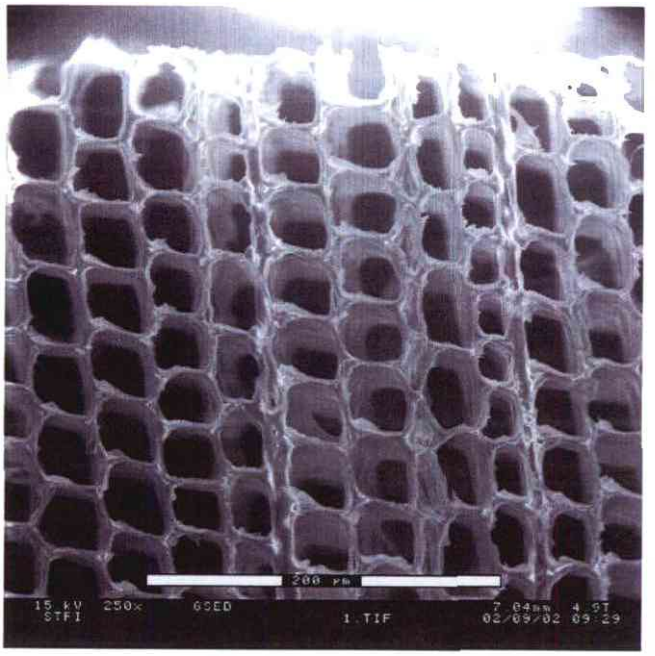

Figure 16. ESEM image of a part of the measured zone in the Scots pine heartwood. The image shows the wood structure across the grain, magnification 250x. In this image it can be observed that the measurements have been made in the early wood.

Figure 16 shows an ESEM image of a part of the measured zone in the heartwood surface layer. In the image it can be observed that the measured zone only consists of early heartwood. The densities in the early wood were measured in the image to 361 kg/m^3 by dividing cell wall area over area of holes and multiply with 1500 kg/m^3, which is the cell wall density. The uncertainty in this measurement is estimated to ± 15 kg/m^3 due to the accuracy in the used method.

In the case of heartwood a measured profile for a rubber bung was used for normalising the measured profiles. The profile of the MR signal in the rubber bung is known as flat. The accuracy in the moisture content profiles for heartwood is dependent on the method used for calibrating the normalised measured signal. The MR profile intensity was converted into moisture content using the known values for initial bulk moisture content and the equilibrium moisture content. The equilibrium moisture content at used climates was found in Esping[38]. The recorded mean signal intensity at 0 and 5 minutes between 335 to 377 µm was used for calibrating against the initial moisture content, 70.5%, and the mean signal at 894 and 1254 minutes at 0 – 84 µm was used for calibration against the equilibrium moisture content, 9.9%. A linear correction was made between the two calibration points. When calibrating the moisture content (kg/m^3) the local density in the surface layer was used for wood and the measured bulk density for concrete. The local density in the Scots pine sample was measured in the ESEM image as described above

[38] Esping, B. 1992. Grunder i trätorkning, 1a. *In Swedish*. Trätek, Stockholm, 234 p.

5.1.2 Spruce

The results from the spruce measurements were difficult to analyse due to problems with noise in the measurements and problems with levelling the sample. This has been further investigated and attempts made to fit the data to a single exponential function in Excel. Magnitude data was used because the data could not be satisfactorily phased across the whole width of the sample using zero and first order phase correction. The base line noise level was subtracted to correct for the systematic error in taking magnitude data. The data points were cut when they fell below the baseline noise level. The fit of this data gave a T_2 of 1 to 3 ms but was subject to errors of around ± 50% this data is shown in figure 17. The T_2 appears to decrease as the experiment is repeated over time and water is lost from sample as expected. However this would also be true when fitting data which has a decrease in the signal to noise ratio over time. There is also a huge variation at the edges of the sample due to the very low signal intensity.

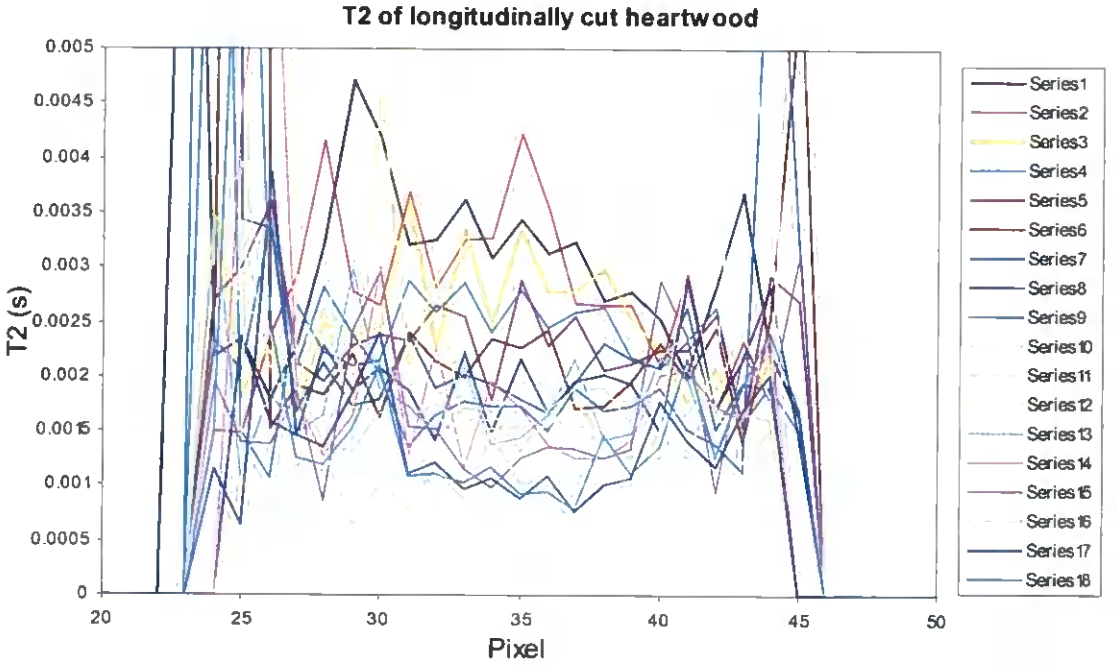

Figure 17. T2 values found from a single exponential fit for the longitudinal spruce heartwood at each pixel position through the sample.

The initial intensity profiles determined from the same fit shown in Figure 18 are reasonable but are subject to a higher noise level than the average intensity profiles. They are not significantly different from the average intensity profiles already provided. The fits are only carried out until the 18th data file when the signal to noise ratio becomes too small to give statistically viable fits.

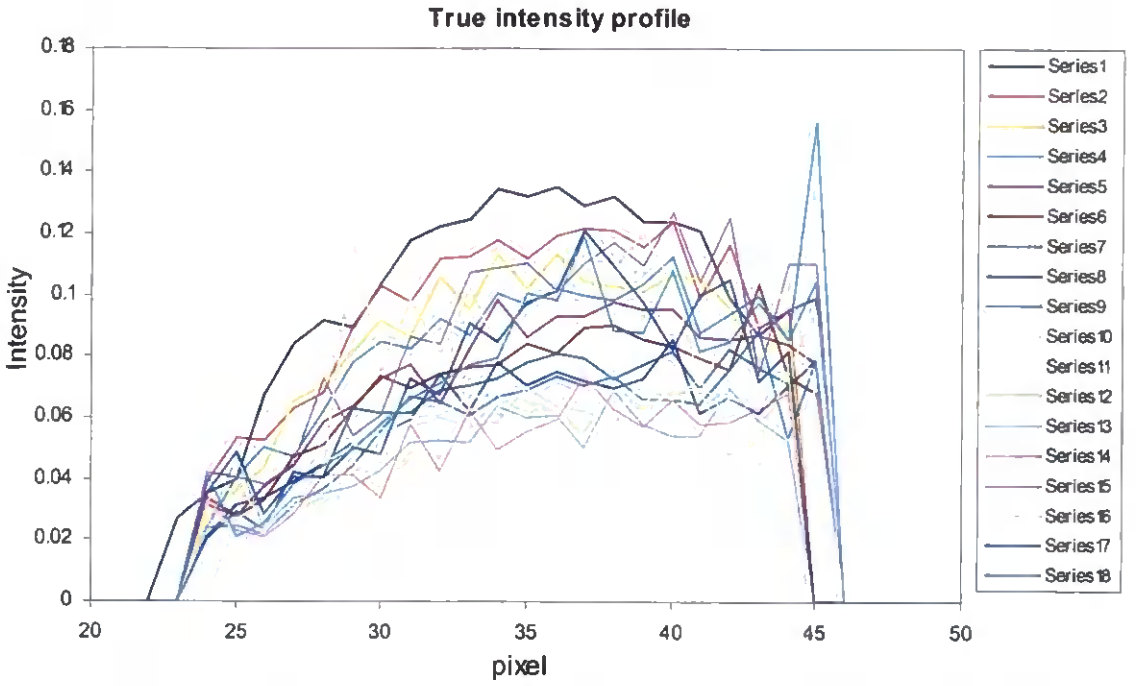

Figure 18. Intensity profiles calculated from a single exponential fit at each pixel position across the sample.

In figure 18 it can also be seen that there is no sharp edge in the measured values at the surface interface. This is most probably due to bad surface alignment with the magnetic field. In the case with the Spruce experiments the probe was aligned with the magnetic field prior to the first measurement. This was not good enough since each wood samples were not identical in shape. In the case with Pine most of the sample surfaces was aligned with the magnetic field before the measurement started. During this period the airflow was set to zero and no change in the signal amplitude could be seen during the time for levelling the probe accurate which typically could take 5 to 10 minutes

5.2 GARField profiling of aqueous coatings

5.2.1 Samples F and S.

Results are presented for the water ingress and egress for test samples F2, F3, S1 and S2. They were held on a wet sponge outside the instrument for 120 hours for the water ingress. Samples were dried in a desicator over silica gel for 48 for water egress. Samples were dried on a paper towel weighed and transferred on to the thin film coil for measurement. Measurements were made for forward and backward transport and for each end of each sample.

The results clearly showed ingress and egress of water through the wood and coating and clear differences between the two coatings. The coating on sample 'S' was seen to give a much higher intensity and become thicker after taking up water than sample 'F'. This increased signal was rapidly lost from the coating sample 'S' on drying. Sample 'S' had a step in the intensity profile from the coating, which remained during the entire experiment. The reasons for this step are not yet known. Sample 'S' became slightly 'tacky' when wet as it adhered slightly to the glass cover slips.

The baseline (starting) profiles of the four samples are shown in figure 19. The detector coil is to the left of the window. The signal from the coating is seen to fall between 300 and 700 μm with all the coatings giving a signal of different thickness. The normalised intensities are all very similar. While the 'F' samples give a square edge the 'S' samples show a step in the intensity which may indicate that the surface is not smooth or that the surface has a different characteristic to the bulk. Again this step shows a similar intensity for each of the 'S' samples. To the right of the coating is seen a very small signal intensity from the wood substrate.

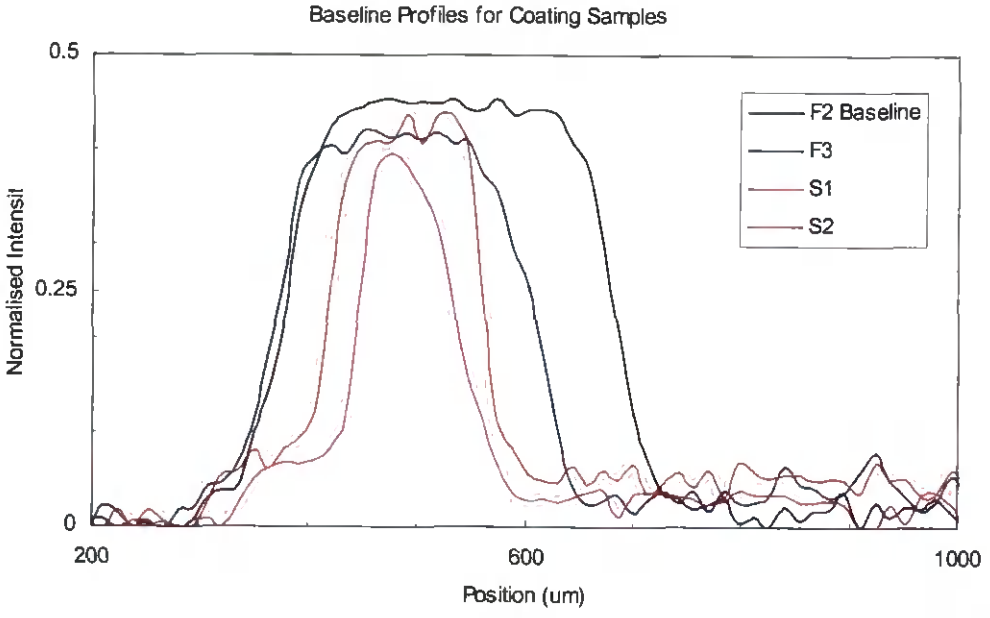

Figure 19. Baseline profiles for the coating samples. The detector coil is to the left of the window. The large intensity in the centre is from the coating layer while the wood substrate is to the right.

5.2.2 Acrylic paint

Sample "F" was test samples coated with coating "F", a water-borne commercial acrylic paint containing surface-active substances. The water proton intensity profiles obtained from sample "F2" are shown in figure 20 (ingress of water) and figure 21 (degress of water). The coating/air interface starts at approximately position 400 microns at the beginning of the water ingress phase. From approximately position 750 and upward is the wood substrate.

The black crosses mark the baseline profile. The signal intensity is seen to be increasing in the wood on the profile taken at 6 hours and has continued to increase on all the measurements. The signal intensity in the wood appears to be parallel to the baseline for all measurements. This shows the relatively fast diffusion of water through the wood substrate. The signal in the coating at 2 hours first increases on the wet side. At 6 hours the increase in intensity is fairly constant over the whole coating thickness. The intensity decreases in the measurements taken at 24 and 54 hours before increasing again at 120 hours. This may be within the noise of the measurement. The coating appears to have got slightly thicker, by around 100 μm during the experiment.

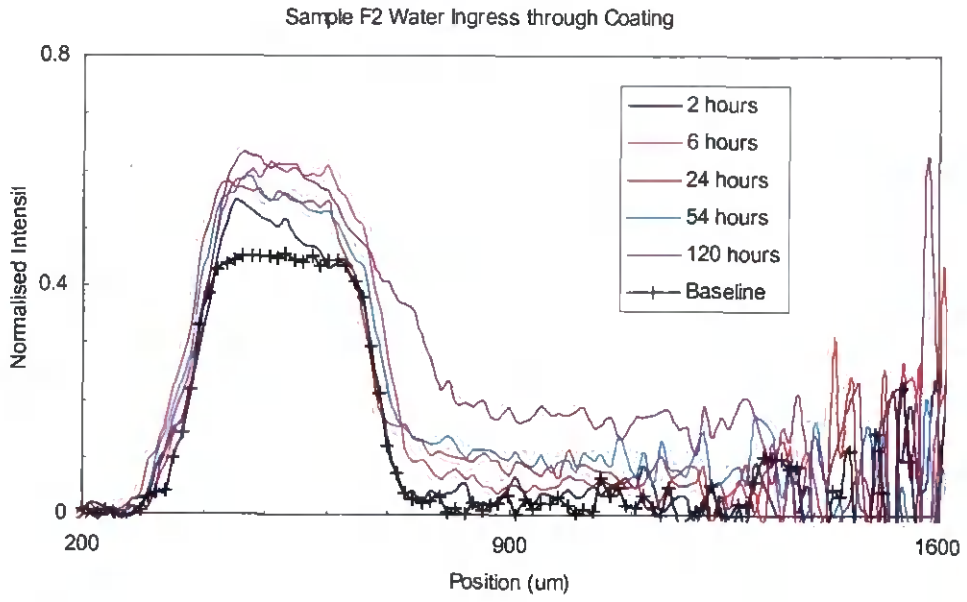

Figure 20. Profiles of coating sample 'F2' during water ingress experiment.

The water egress through sample 'F2' is shown in figure 21. The signal in the wood decreases on each profile to its original level after 48 hours. The signal intensity in the coating is a minimum at 24 hours before increasing again at 48 hours. The signal intensity in the coating at 48 hours is left with a slope on the wood side of the coating. The thickness of the coating region shows approximately the same thickness as the baseline (shown by the black crosses).

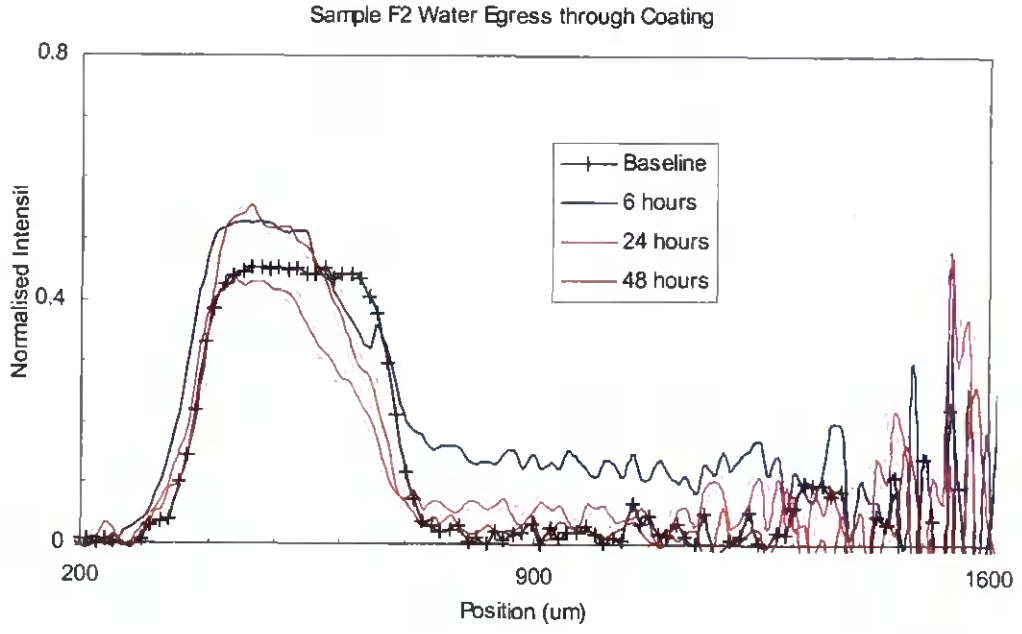

Figure 21. Profiles for water egress through coating sample 'F2'.

Substituting the baseline intensity from the 120 hours intensity yields a measure of the water accumulation versus depth from coating/air interface. The result is shown in figure 22. It is interesting to notice the maximum at approximately position 750. It correspond to the position of the coating/wood interface.

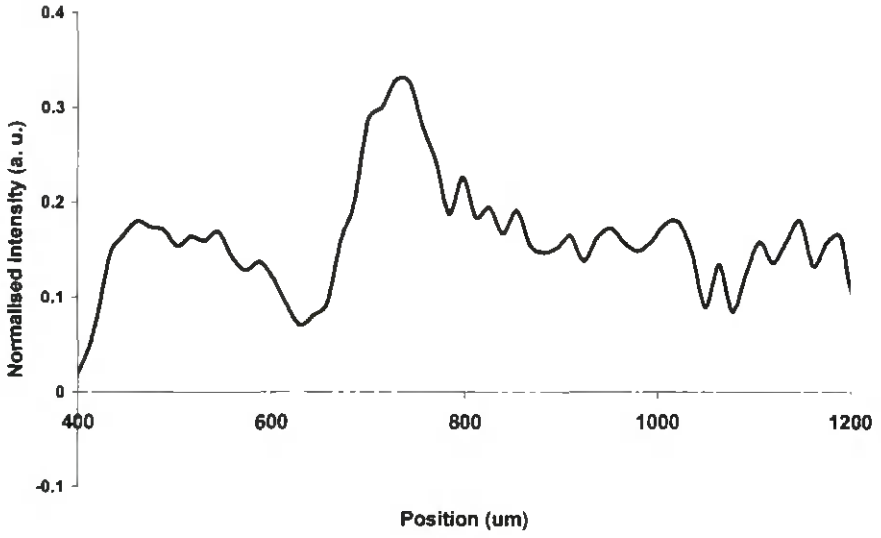

Figure 22. Water proton density as function of distance from coating/air interface.

Figure 23 shows an ESEM image of the coating "F2" to the left (coating thickness approx. 350 µm) applied to wood. The water proton density profiles (green reference profile and red exposed to water) has been superimposed on an ESEM image of the area where the MRI measurements were carried out. The water proton density is proportional to the moisture content. It is clearly shown that an accumulation of moisture occurs at the interface between coating and wood, at "distance 750".

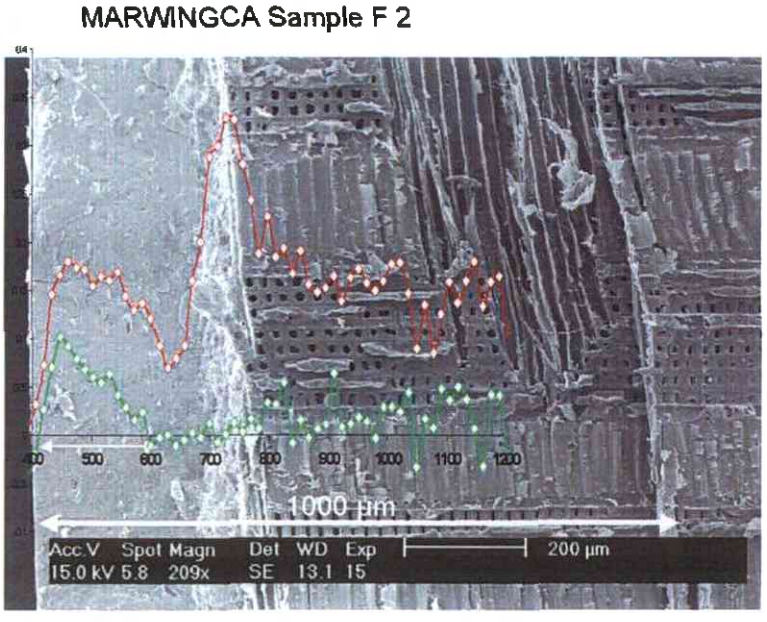

Figure 23. ESEM image of sample "F2" with proton density profile.

The water proton intensity profiles obtained from sample "F3" are shown in figure 24 (ingress of water) and figure 25 (degress of water). The coating/air interface starts at approximately position 350 microns at the beginning of the water ingress phase. From approximately position 650 and upward is the wood substrate.

Profiles of sample 'F3' were measured after the coated surface had been in contact with the wet sponge. The intensity of the coating is very similar to that shown by 'F2' but appears to stay much more uniform over time. The profile changes completely for the measurement at 120 hours possibly due to lifting of the coating from the wood, at position 750. This effect is still present at 6 hours into the drying as seen in figure 25 but is lost at longer times. The intensity profile in the wood coating also changes significantly at 120 hours showing a large slope, the reasons for this are unknown at this time. The data shown in figure 25 for the drying stage also like 'F2' show a differently shaped final profile to the original baseline measurement.

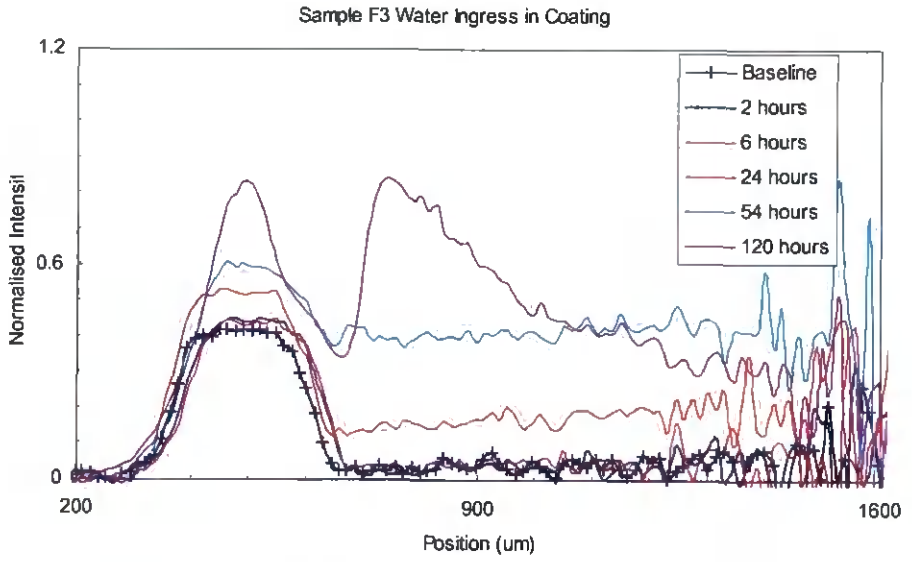

Figure 24. Profiles of coating sample 'F3' during water ingress experiment.

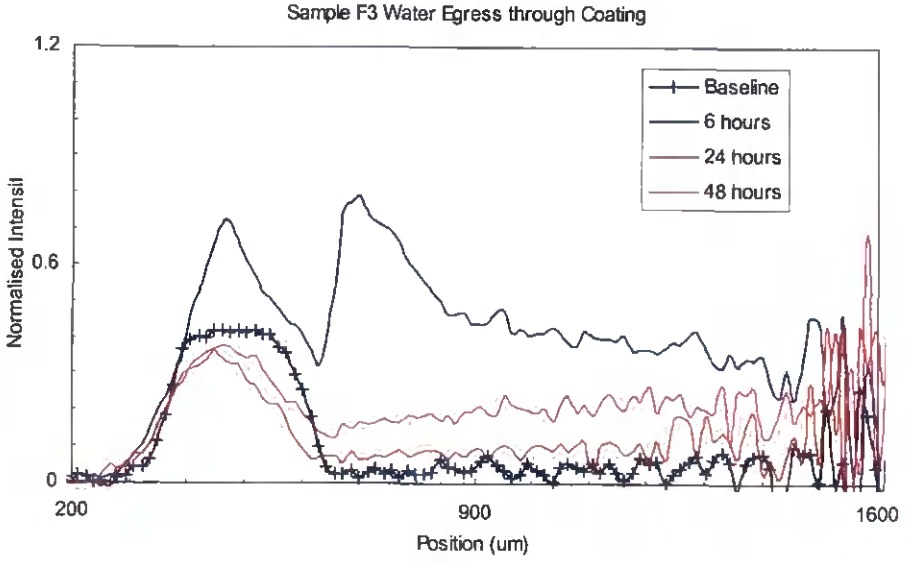

Figure 25. Profiles of coating sample 'F3' during water egress experiment.

5.2.3 Alkyd emulsion paint

Sample "S" was test samples coated with coating "S", a water-borne commercial alkyd emulsion paint containing surface-active substances.

The water proton intensity profiles obtained from sample "S1" are shown in figure 26 (ingress of water) and figure 27 (degress of water). The coating/air interface starts at approximately position 350 microns at the beginning of the water ingress phase. From position 600 and upward is the wood substrate.

Profiles of sample 'S1' were measured after the coating was in contact with the wet sponge. These profiles show a much greater intensity increase in the coating layer than sample 'F'. They also show a greater increase in the thickness, probably due to greater tendency to accumulate water. The shoulder on the left of the coating remains and also increases in intensity with water uptake. There appears to be a slope towards the coating in the signal intensity in the wood, which was not so evident for sample 'F'. Profiles taken during the drying stage are shown in figure 27. These show that the signal intensity is lost very rapidly from the coating. In fact it is below the baseline measurement within 6 hours. This indicates that the drying of the coating layer is a fast process. The final profile after 48 hours of drying is slightly thinner than the original measurement for the coating region. The signal intensity from the coating has dropped to about half its original value, however the shoulder has the same intensity.

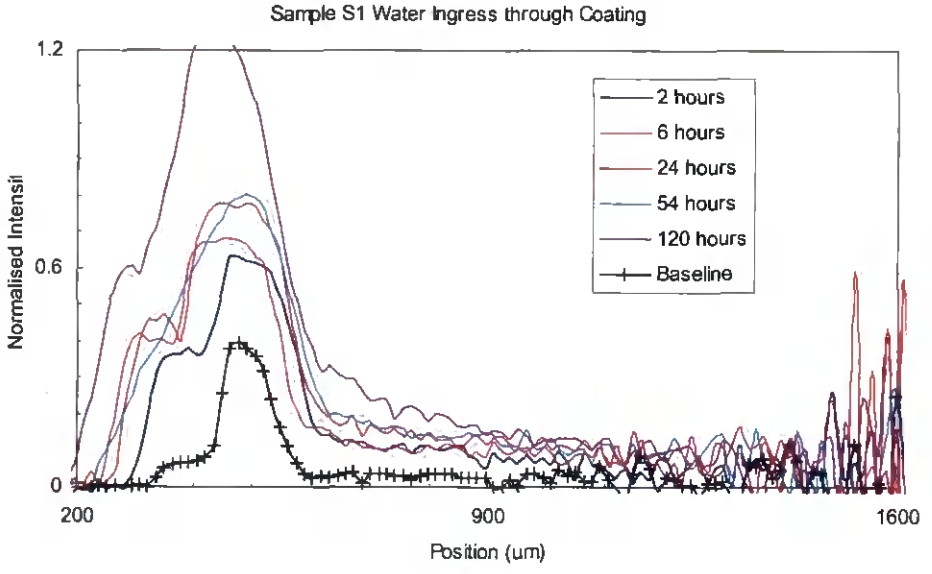

Figure 26. Profiles of coating sample 'S1' during water ingress experiment.

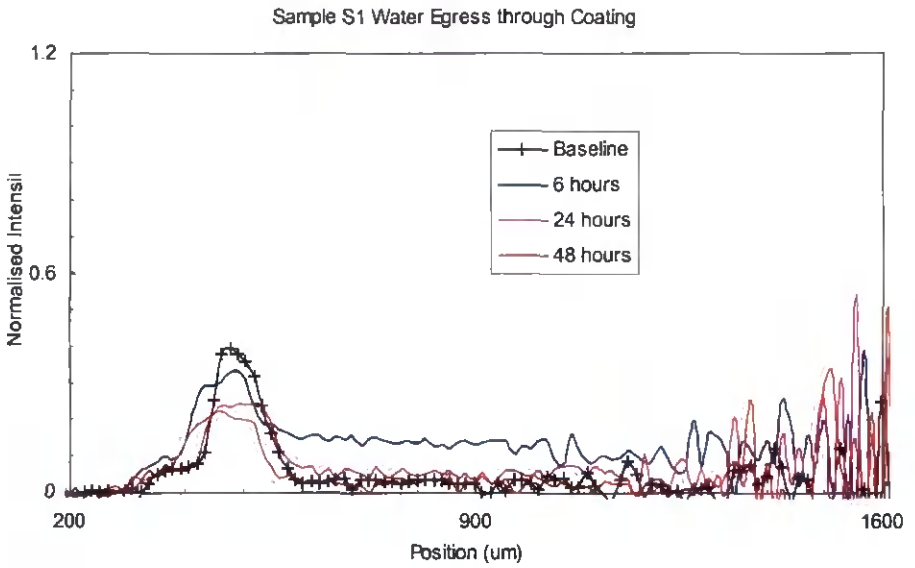

Figure 27. Profiles of coating sample 'S1' during water degress experiment.

The drying profiles shown in figure 27 show a rapid decrease in intensity. Even after 6 hours of drying the profile is below the baseline profile. This indicate that the drying of the coating layer is a fast process and that the coating does not contain substances that to great extent retards the evaporation of water and moisture during desorption.

The water proton intensity profiles obtained from sample "S2" are shown in figure 28 (ingress of water) and figure 29 (degress of water). The coating/air interface starts at approximately position 300 microns at the beginning of the water ingress phase. From position 600 and upward is the wood substrate.

Figure 28 shows that the coating intensity increases much slower than for the sample 'S1' and the signal intensity in the wood after 120 hours is greater. The drying profiles shown in figure 29 shows a rapid decrease in intensity as also is seen for sample 'S1'. Again the final profile taken after 48 hours of drying is smaller than the original profile.

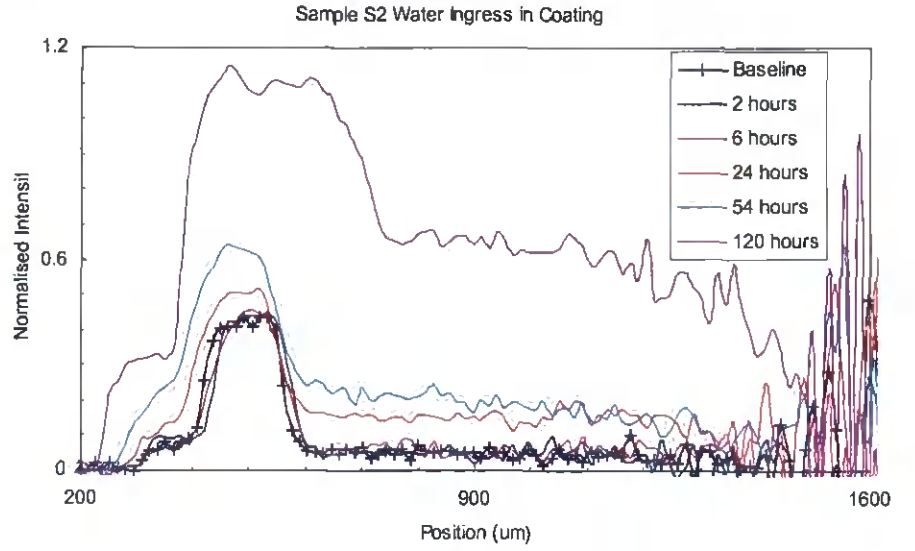

Figure 28. Profiles of coating sample 'S2' during water ingress experiment.

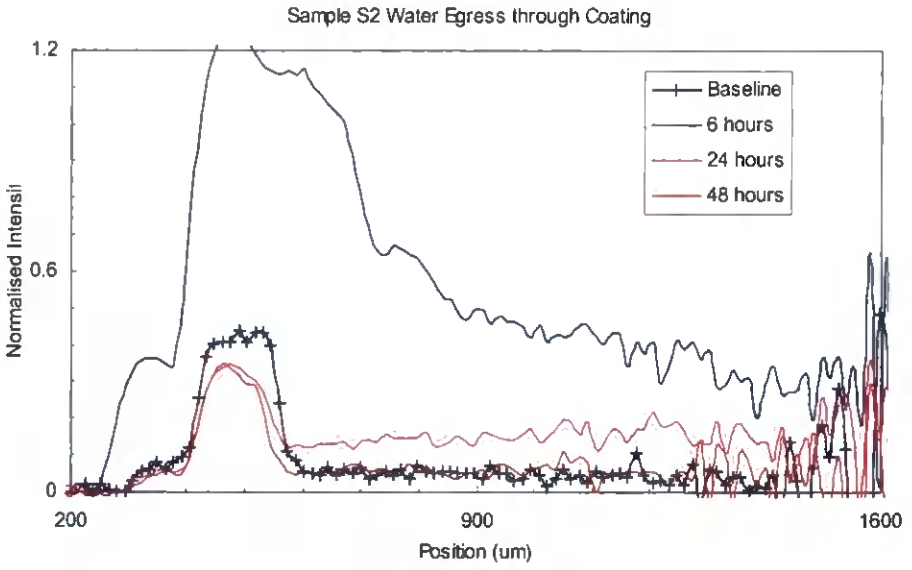

Figure 29. Profiles of coating sample 'S2' during water egress experiment.

It is quite obvious that sample "S2" show large accumulation of water behind the coating layer as indicated by the high profile in region 600 to 1300 microns.

5.2.4 Internal Comparison Product

- Sample "ICP1".

The water proton intensity profiles obtained from sample "ICP1" are shown in figure 30 (ingress of water) and figure 31 (egress of water). The coating/air interface is approximately at position 300. From approximately position 500 and upward is the wood substrate. With the coating nearest the coil, there is an increased signal intensity for approximately 300 microns on the edge of the sample. This increases steadily in amplitude, but not depth, as the sample is wetted. This region is most likely assigned to the coating. Beyond this the signal intensity also increases over time. In the 24 hours of drying the profile returns to a similar intensity as the starting profile. In the drying stage, figure 31, there is a decrease to the baseline in around 24 hours. At a depth of around 700 microns into the wood there is an apparent increase in the signal intensity before the increase in noise becomes significant. The reason for this increase is not understood but is thought to be due to the different structure in the growth rings of the wood. This sample has growth rings of around 1 mm parallel to the sample surface.

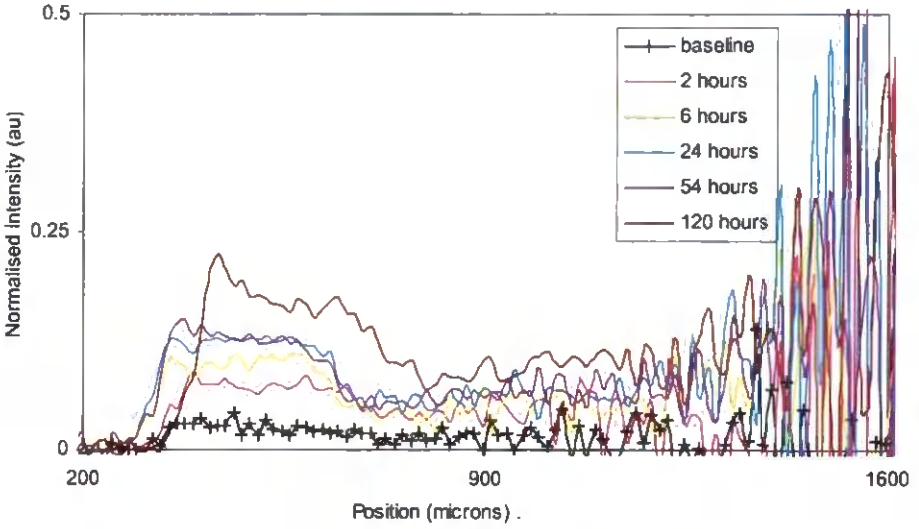

Figure 30. Profiles of water ingress through the sample ICP1.

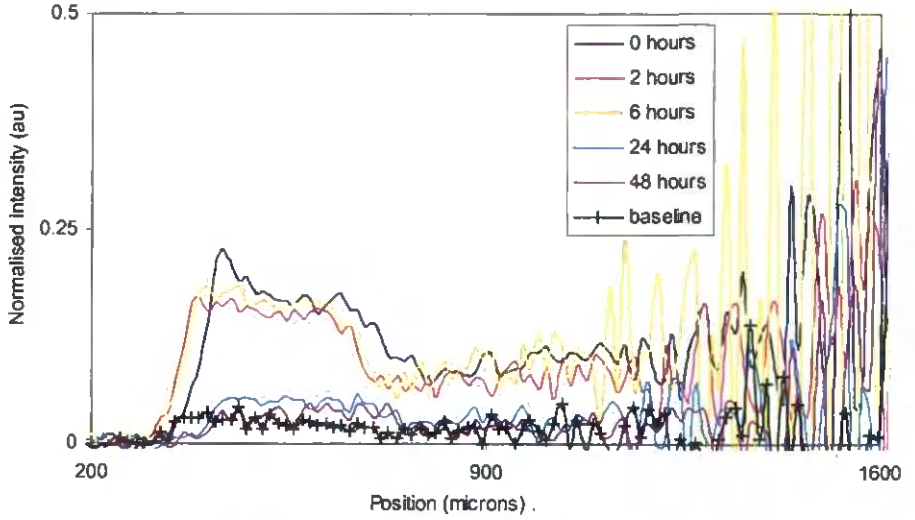

Figure 31. Profiles of water egress through the sample ICP1.

5.2.5 Polyurethane

- **Sample "PU1".**

The water proton intensity profiles obtained from sample PU1 are shown in figure 32 (ingress of water) and figure 33 (egress of water). The coating is approximately at position 300 to 450 microns. From position 450 and upward is the wood substrate. The profiles indicate a relatively uniform moisture distribution through the coated test sample. The profiles appear to have a similar intensity throughout the coating and wood.

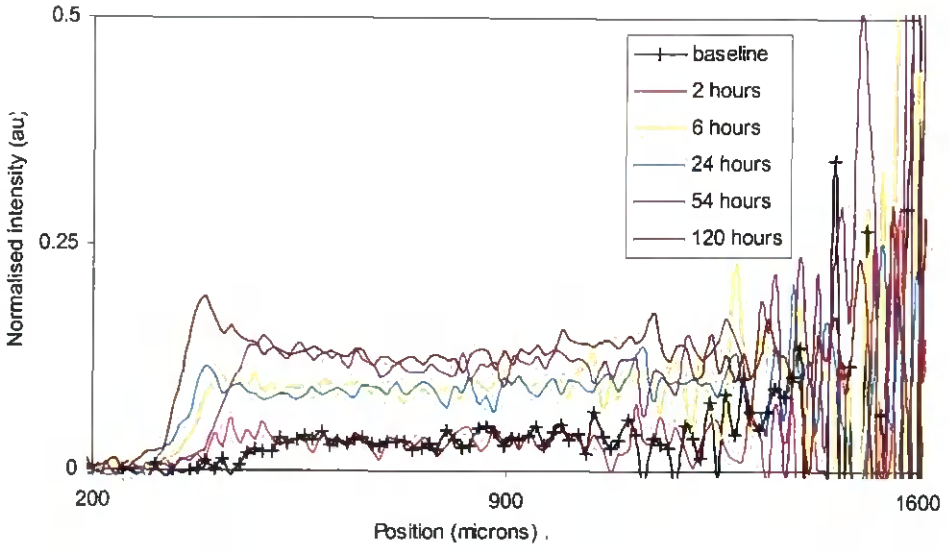

Figure 32. Profiles of water ingress through the sample PU1.

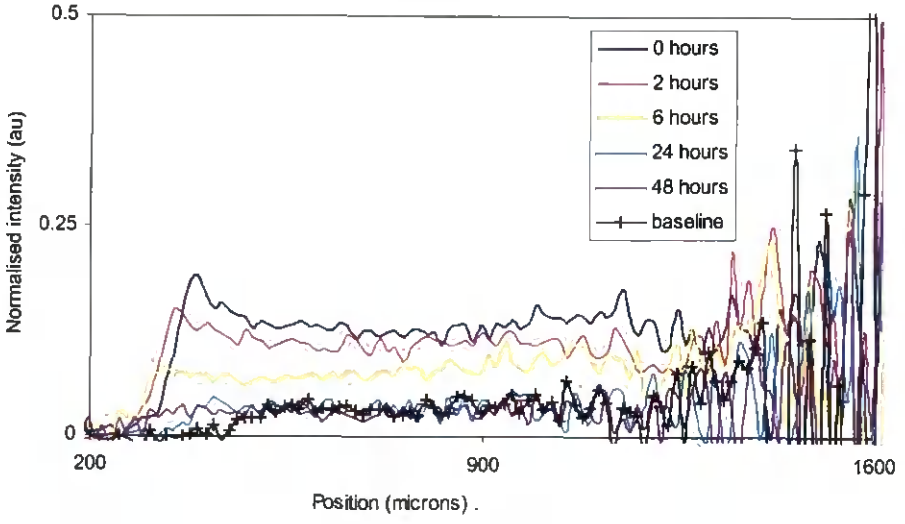

Figure 33. Profiles of water egress through the sample PU1.

The polyurethane coating seems to keep the moisture content at a low level. This coating shows a water absorption value of 150 g/m^2 tested according to European standard EN 927-5.

5.3 GARField profiling of glued interfaces

5.3.1 Glue curing

Exemplar profiles obtained during glue cure are shown in figure 34. These profiles were obtained for pine glued to glass with UF. The radio frequency coil is at 0 μm on the position scale. It is followed by the signal from the Mylar marker tape at around 250 μm. The Mylar has a constant intensity and position. There is very little signal between 300 and 900 μm which corresponds to the lower layer of wood which contains insufficient mobile ^{1}H to be readily visualised even with $\tau = 70$ μs. The strong signal intensity centred at around 950 μm is due to the mobile ^{1}H of the glue. The glass cover slip is between 1000 and 1100 μm. Beyond

1100 μm the signal comes from the elastomer. The intensity of this signal decays with distance from the surface coil. The glue line signal decreases on each successive profile and the decrease can be used to estimate the cure time. The position of the lower edge of the elastomer changes with time as the wood and glue layer first shrinks and then (see below) swells.

The time taken for the glue line signal to fall to half the intensity recorded in the first profile is taken as a measure of the glue cure time. The first profile is available 8 minutes after the bond is made. While it is appreciated that the signal intensity must decrease significantly in these first few minutes, this measure of cure time is, nonetheless, a significant indicator of glue performance. The hardener 2508 cures slightly faster than the standard (hardener 2553) while hardener 2580 cures significantly more slowly. These trends are in general accord with the published working times of the glues. If the wood and glue is pre-heated to 70°C immediately before measurement, then a much quicker cure is seen, presumably since crosslinking is thermally activated. However, prolonged storage of the glue outside the manufacturer's recommended temperature range produces a longer cure time, due to an increase in the viscosity of the glue. Varying the fraction of hardener up or down results in a slightly faster cure while increasing the thickness of the glue layer produces a longer cure time as might be expected since the water takes longer to diffuse from the glue. Finally, if the wood is changed from pine to spruce, the cure time is increased presumably because of differences in the microstructure of the wood. Pine has a long cells with an open structure whereas spruce has shorter cells more difficult for water to ingress[39].

The position of the elastomer edge for the data set recorded is shown in figure 34. The edge position shows that that the sample (pine - UF- glass) thickness decreases for the first 100 minutes before subsequently increasing, finally reaching an equilibrium value after about 1000 minutes. The thickness change reflects changes in the distribution of water in the sample. During the first 100 minutes, water is lost from the glue by diffusion into the wood. This is seen from the MR measurements by an increase over the same period in average signal intensity in the wood layer, figure 35. After 100 minutes, the signal intensity in the wood begins to fall indicating either a change in the mobility of the water or a loss of water due to evaporation. Evaporation is not considered important, first since the wood and glue are sandwiched between glass slides and second because the overall thickness of the sample once again increases. One possible explanation is that the water, which initially diffuses rapidly into the wood, first occupies small otherwise air filled pores where it is mobile. With time the water is absorbed into the wood fibres causing them to swell[39]. The water becomes bound into the structure with a reduced mobility giving a reduced MR signal

5.3.2 Glue curing: Loss of water

5.3.2.1 Chemical hardening without solvent loss

When glue is placed between two glass cover slips, there is no loss of water neither to the air nor to the substrates, which is illustrated by that the thickness doesn't decrease but can also be verified though weighing. In figure 34, the hardening of UF glue between two pieces of glass is monitored.

---

[39] Jane FW, The structure of wood, London: Black, 1970.

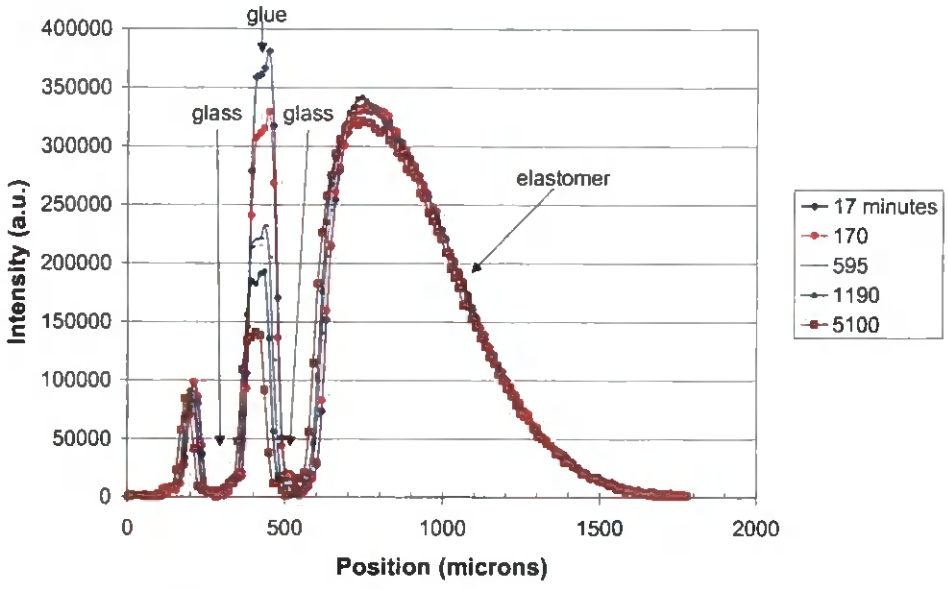

Figure 34. Profiles of glass-glue-glass during cure.

The NMR signal of the glue between 390 and 470 µm is fairly uniform with a tendency to water gathering towards the upper substrate. The glue line thickness is constantly 80 µm throughout the experiment, which confirms that water is not let out. In figure 35, the development of the NMR signal with time is shown.

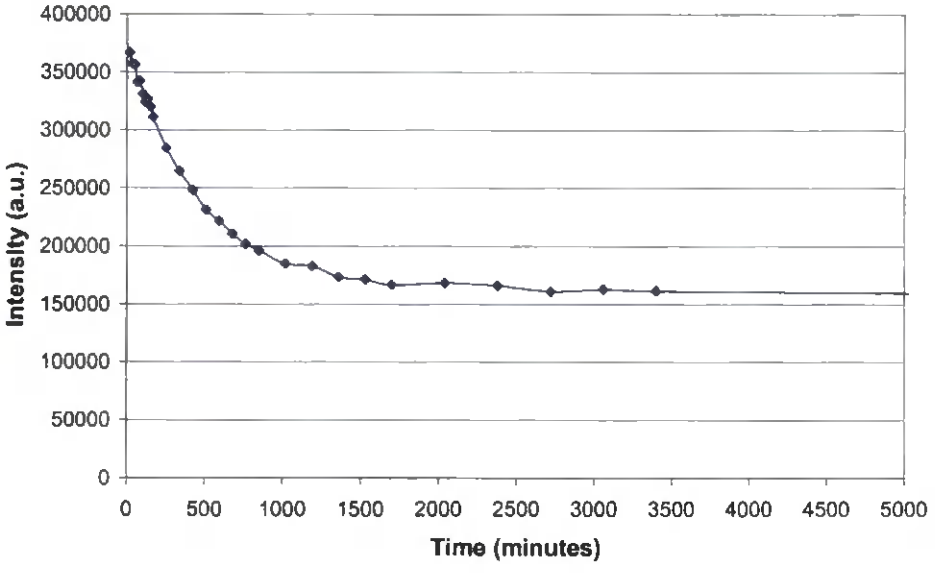

Figure 35. Decrease in glue signal intensity over time.

The NMR signal is decreasing exponentially with time and reaches a plateau after around 1000 minutes when the NMR signal has been reduced to half of its initial intensity. This suggests that a chemical hardening has been taken place as the water cannot disappear and that water stands for less than half of the initial mobile proton density. Possibly the chemical hardening will continue if water is let out, though.

5.3.2.2 *Evaporation to air*

When glue has been placed on a glass cover slip without any upper substrate, the water in the glue will evaporate (see figure 36).

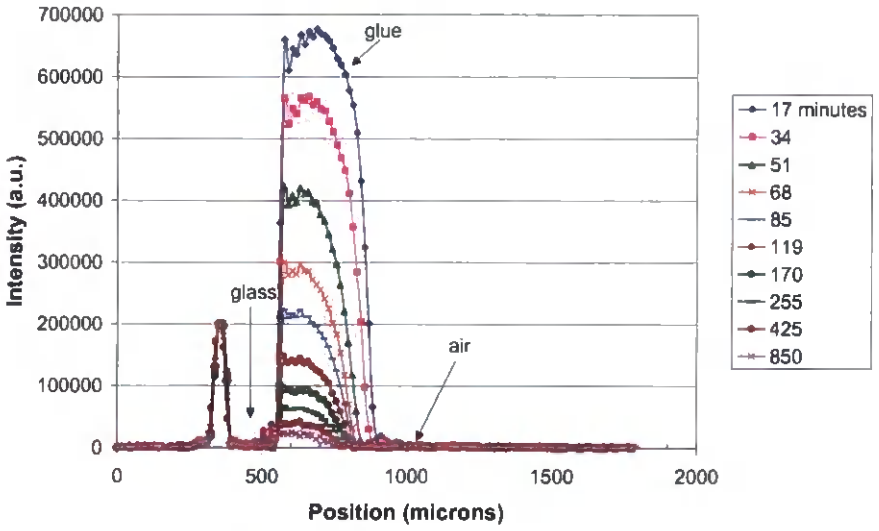

Figure 36. Profiles of glass-glue-air during cure.

In this configuration the NMR signal is reduced both due to chemical hardening and to drying. It is for example readily seen that the glue line thickness is decreased due to drying. The NMR signal on the side of the glue line towards the air is crooked, which suggests that the transport of water from the glue to the evaporation front and out in the surrounding air is limited by the diffusion velocity in the glue line.

In figure 37, it is seen that the NMR signal is quickly reduced when both chemical hardening and evaporation takes place.

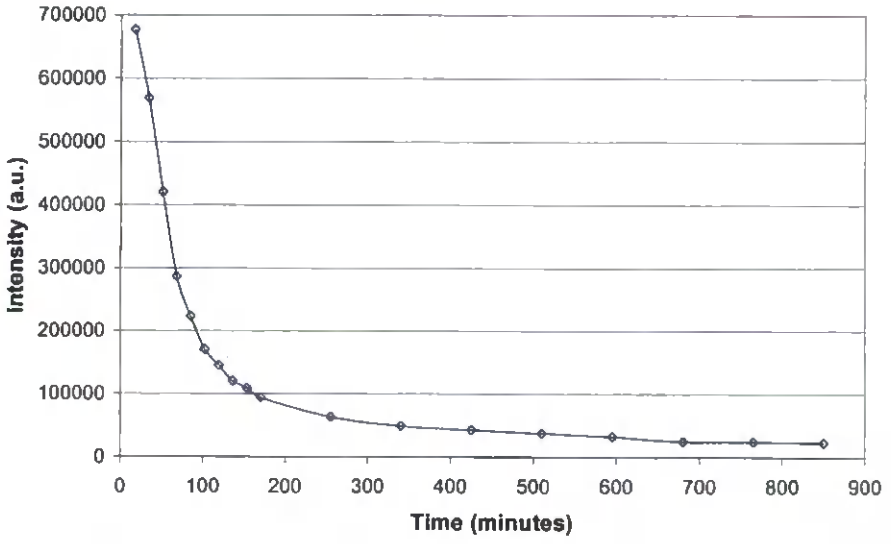

Figure 37. Decrease in intensity of the glue line over time.

Reduction to half height takes 50 minutes in this configuration compared to 1000 minutes for glue between two glass cover slips. In figure 38, it is shown that the glue line thickness decrease is proportional towards time with 1.6 μm/minute until 70 minutes. It has then decreased with at least 80 μm or 25 % of the first measured thickness of 330 μm.

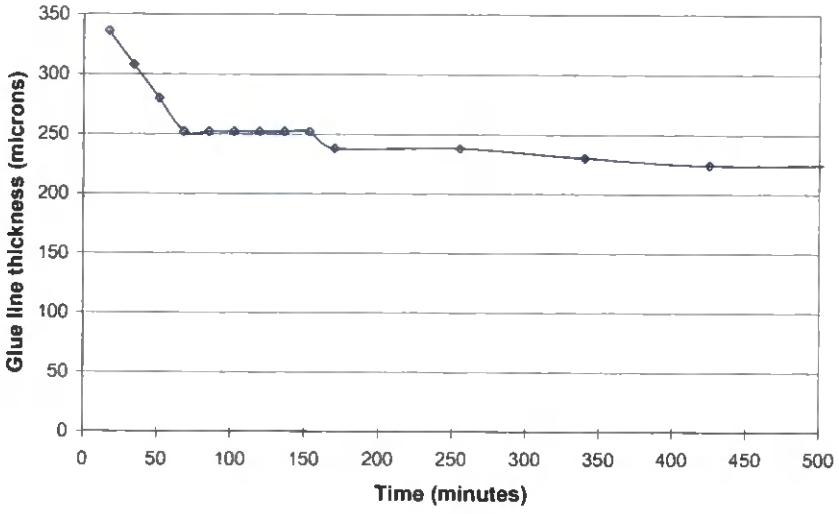

Figure 38. Change in width of the glue line over time.

After 170 minutes it can be seen that the thickness is further reduced. This might be due to that water has been trapped in the glue line due to skin formation and suddenly reaches the surface and evaporates.

5.3.2.3 Water absorption of the wood

When glue is placed between a wood substrate and a glass cover slip, water will be absorbed by the wood substrate. In figure 39, it is shown that the glue signal is reduced, but also that the NMR signal in the wood substrate increases and that the position of the elastomer changes.

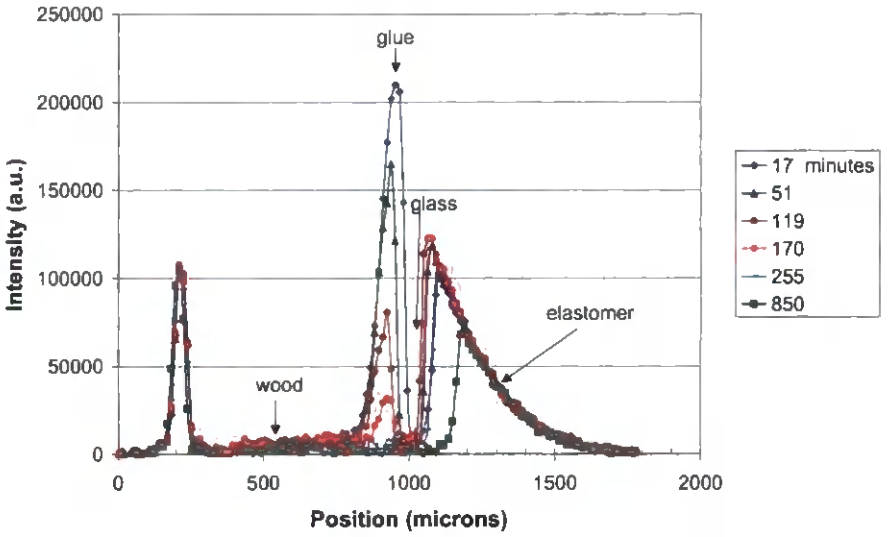

Figure 39. Profiles of wood-glue-glass during cure.

In figure 40, it is shown how the position of the elastomer and the NMR signal or the mobile proton density in the wood substrate varies with time.

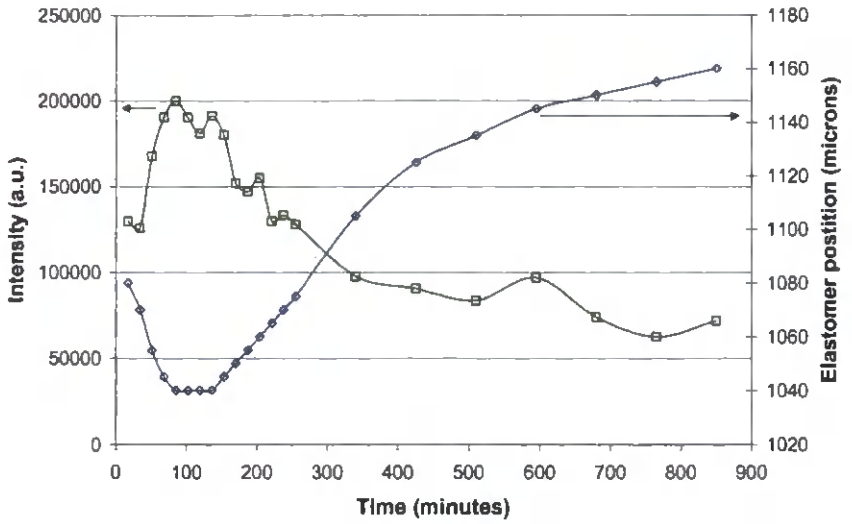

Figure 40. Evolution of the NMR signal in the wood substrate (read on the abscissa to the left) and evolution of the elastomer position (read on the abscissa to the right).

Looking at both curves simultaneously, they mirror each other. The explanation might be as follows: In the first 85 minutes, the elastomer position decreases linearly with time (0.6 µm/minute) as a result of that water from the glue line is absorbed by the wood substrate. This is confirmed by the increase of mobile proton density in the wood. Thereafter the elastomer is raised due to swelling of the wood substrate. This corresponds to a decrease in the mobile proton density in the wood, which probably indicates that the mobile water in the wood cavities are adsorbed by the cell walls and become so tightly bound that they cannot be detected.

In figure 41, the hardening of glue between two pieces of wood is monitored.

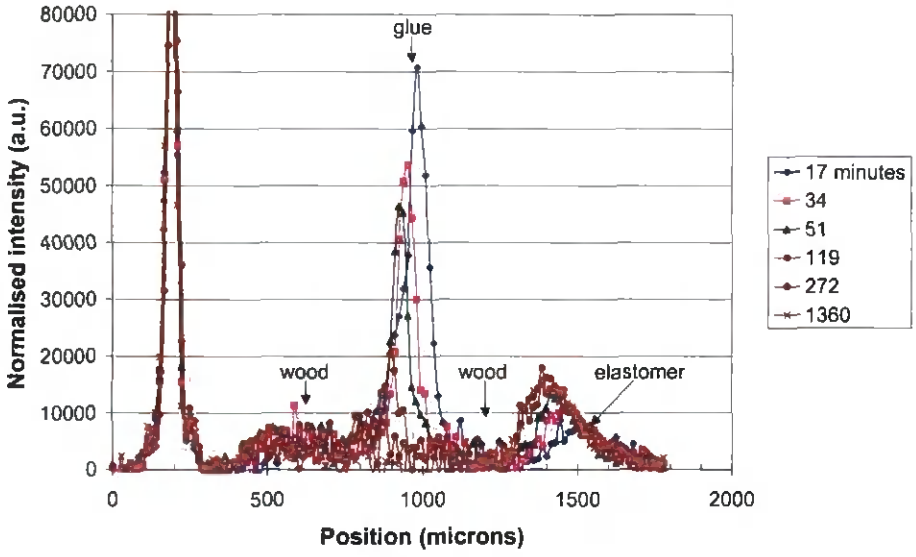

Figure 41. Profiles of wood-glue-wood during cure.

In figure 42, it is shown that the glue line thickness decrease with time with around 1.0 µm/minute. This is almost twice as fast as when glue is absorbed with only one wood substrate, which is quite reasonable.

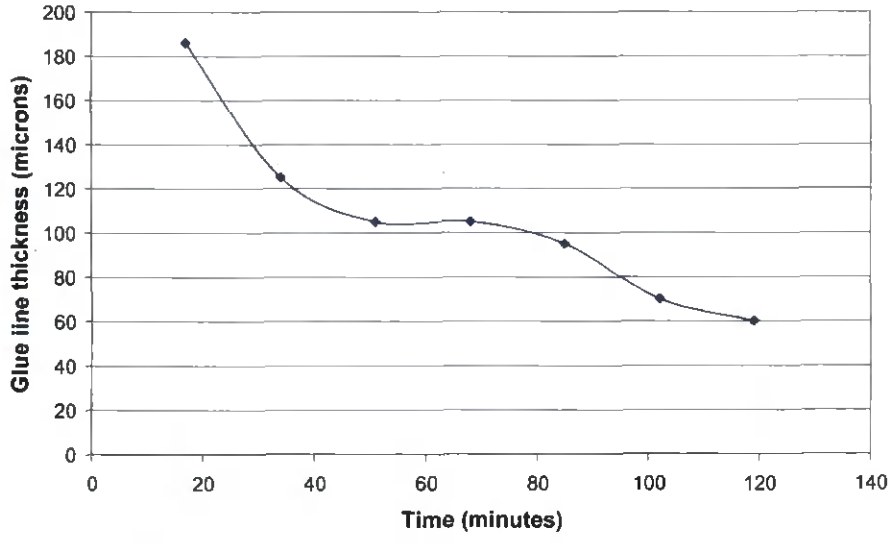

Figure 42. Change in width of the glue line over time.

5.3.2.4 Absorption and evaporation

In figure 43, glue is seen to dry on a wood substrate.

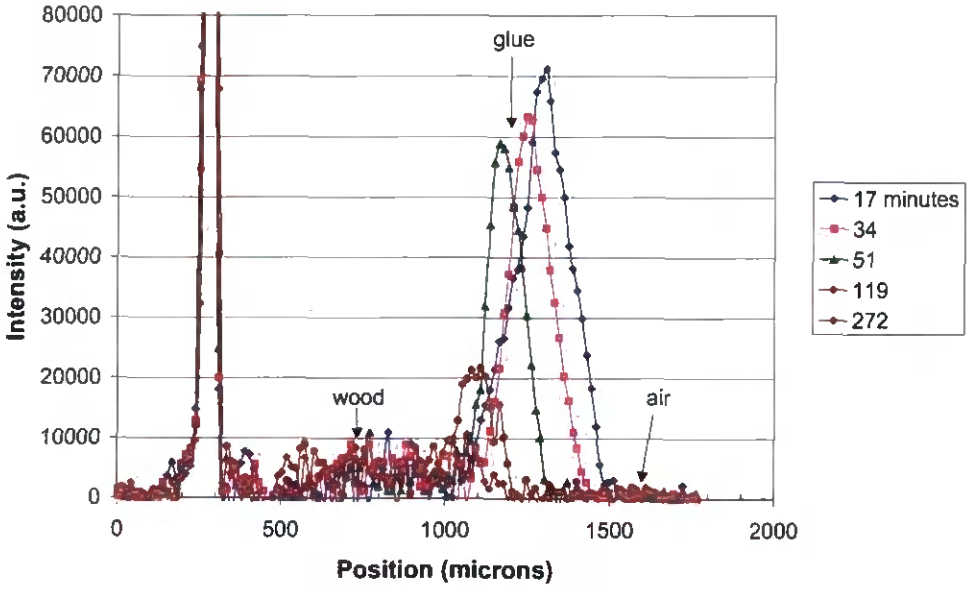

Figure 43. Profiles of wood-glue-air during cure.

During the first 85 minutes, the glue line thickness decrease is almost linear with time, 3.0 µm/minute (see figure 44). This is to high in comparison with the velocities for the glass-glue-air configuration with 1.6 µm/minute and the wood-glue-glass configuration with 0.6 µm/minute, which should be added. However, more replicates might result in a closer value.

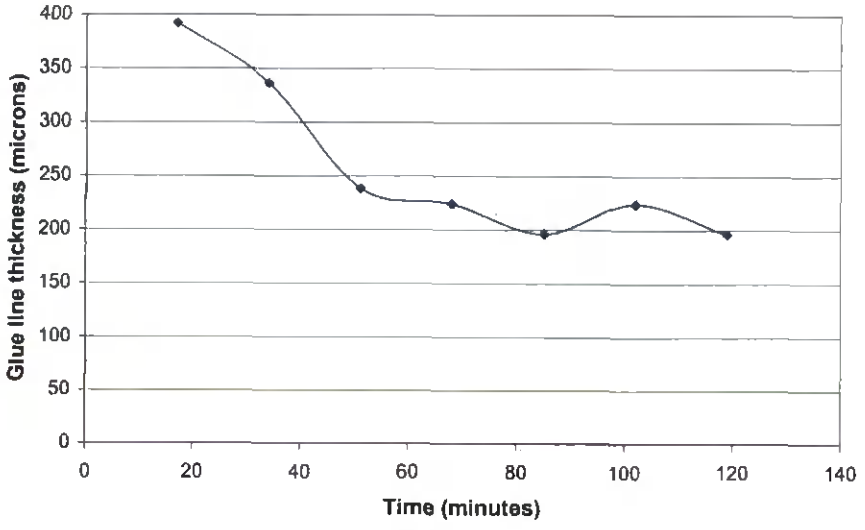

Figure 44. Width of the glue line over time.

During the time measured, the cell walls don't adsorb the water in the wood so that the mobile proton density decreases (see figure 45).

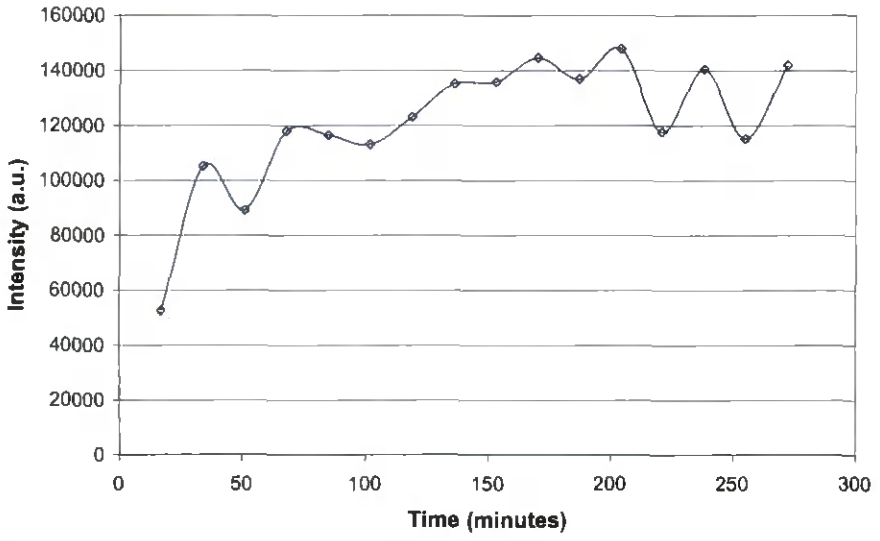

Figure 45. Change in signal intensity over time in the wood substrate.

5.3.3 Glue curing: Hardening time

The loss in intensity of the glue illustrated earlier is mainly due to loss of water from the glue into the wood and reduced mobility of the glue as it cross links. It is therefore an indication of the cure time. The time taken for the glue line signal to fall to half the intensity recorded in the first profile was taken as a measure of the hardening time. The first profile is available 8 minutes after the bond is made. While it is appreciated that the signal intensity must decrease significantly in these first few minutes, this measure of cure time is, nonetheless, a significant indicator of glue performance.

Figure 46 shows how the mobile proton density decreased with time for the standard setting. A certain variation can be identified and therefore the results will be considered as trends.

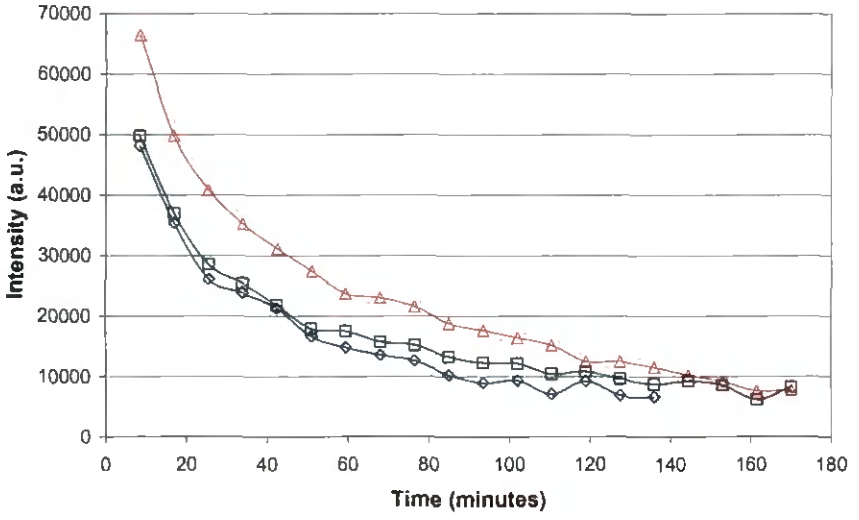

Figure 46. Decrease in signal intensity for three replicates at the standard parameter setting.

In figure 47, the hardening time for three different hardeners is shown. The hardener 2508 cures slightly faster than the standard (hardener 2553) while hardener 2580 cures significantly more slowly.

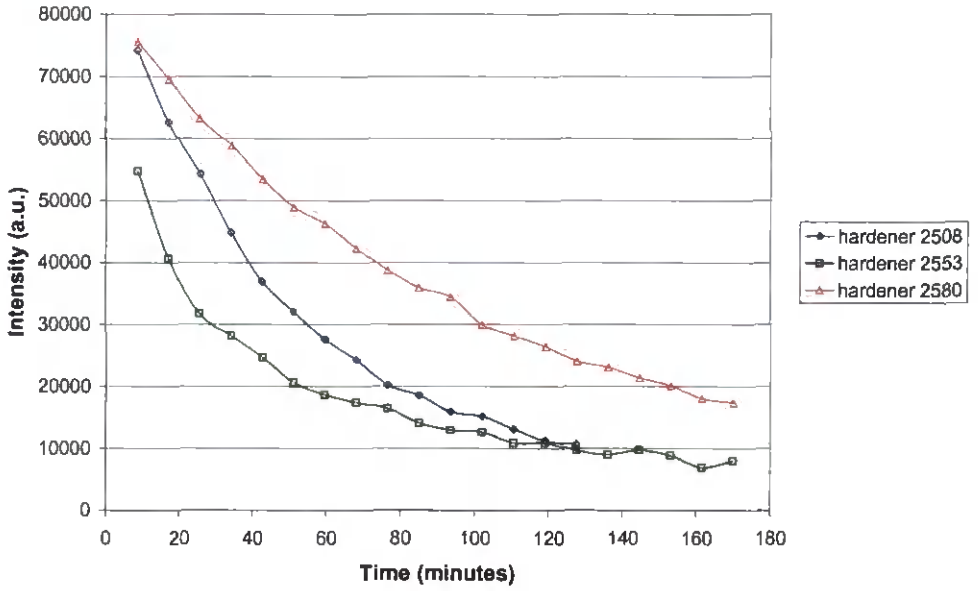

Figure 47. Intensity evolution for the setting glue for different fast hardener types.

Hardener 2553 has been used for all further experiments. Using less hardener (10:100) creates an average loss of signal slightly slower than the 20:100 mix. However a large spread of results is observed in the replicates. By increasing the amount of hardener to 30:100 a slightly faster signal loss is seen (see also figure 48).

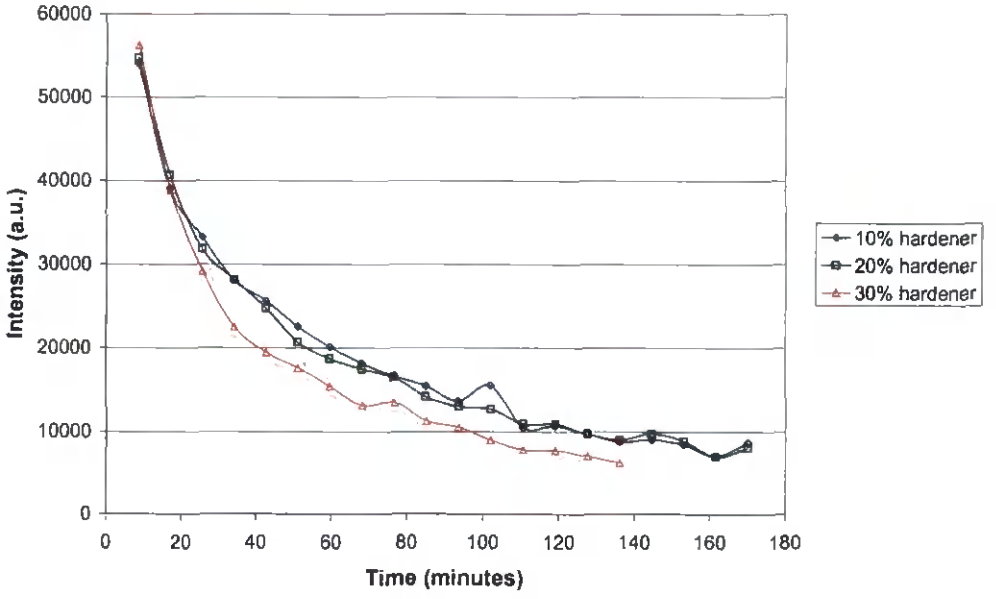

Figure 48. Intensity evolution for the setting glue for different hardener contents.

The glue, hardener, wood and utensils were preheated to 70 °C for 10 minutes prior to mixing. This creates a much quicker loss of signal (see also figure 49).

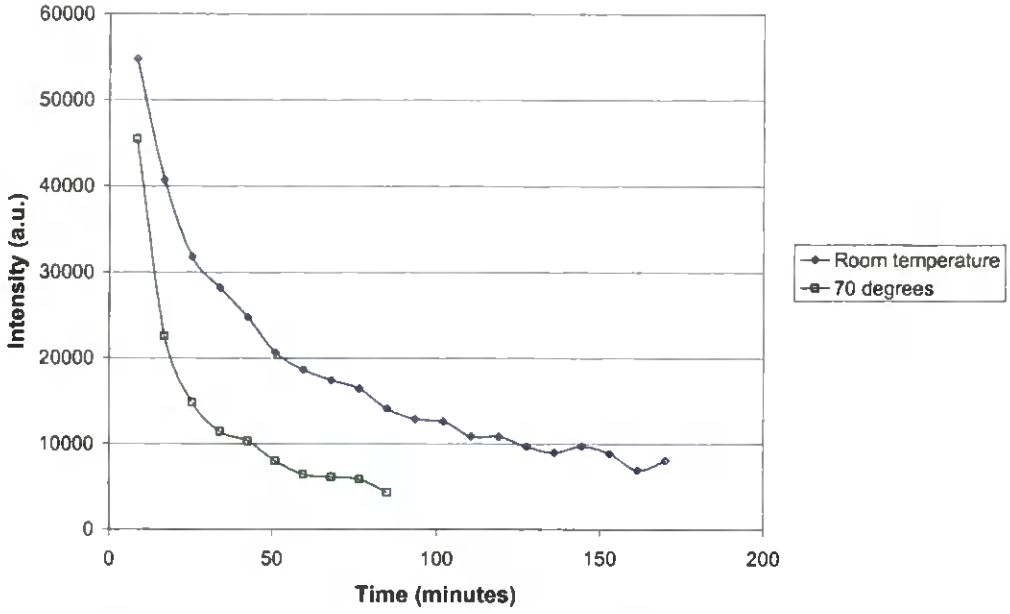

Figure 49. Intensity evolution for the setting glue for different hardening temperatures.

When the glue was spread 300 µm instead of 150 µm there was a large spread of results. The sample preparation probably causes this. In figure 50 it is shown that the average fall in intensity anyway is faster for thinner glue lines.

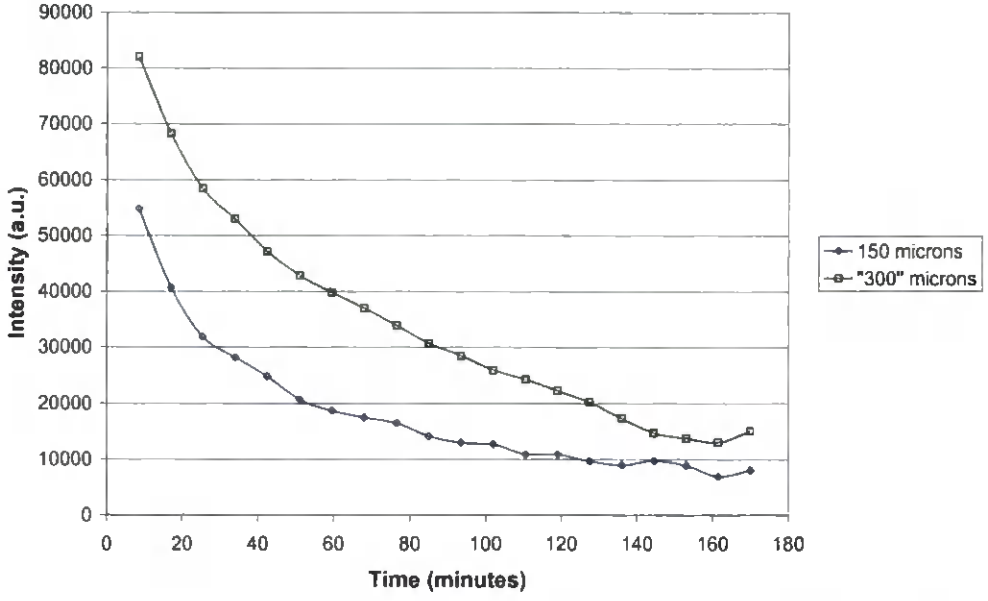

Figure 50. Intensity evolution for the setting glue for different glue line thicknesses.

A portion of the glue was then stored at 34°C for three weeks while the remainder was kept in the fridge at 4°C. There was a large spread of values for these results. The glue stored at 34°C had a much slower loss of signal (see also figure 51).

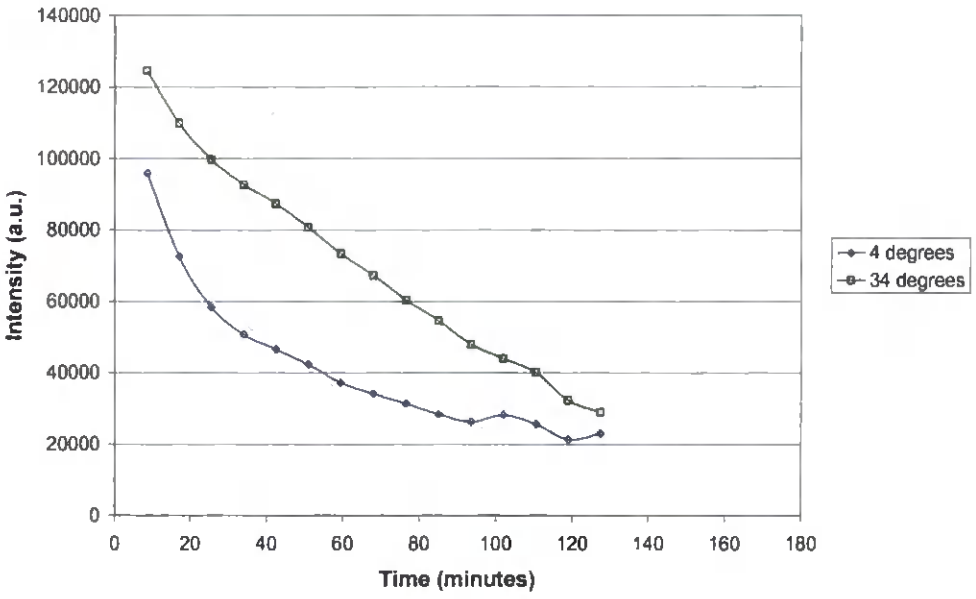

Figure 51. Intensity evolution for the setting glue for different storage temperatures during three weeks.

The diagram in figure 52 shows how the different glue parameters affect the hardening or cure time. We have seen that an increased storage temperature and increased glue line thickness results in a longer hardening time. We also see that an increased hardening temperature and an increased hardener content shorten the hardening time.

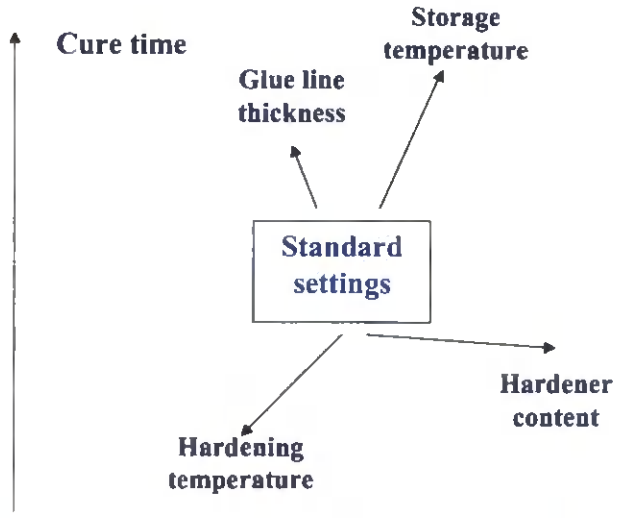

Figure 52. Schematic diagram of how different process parameters affect cure time.

5.3.4 Moisture diffusion

5.3.4.1 Localisation of the glue line

In figure 53, a profile taken with 16000 scans of a PVAc glue line without added water is shown.

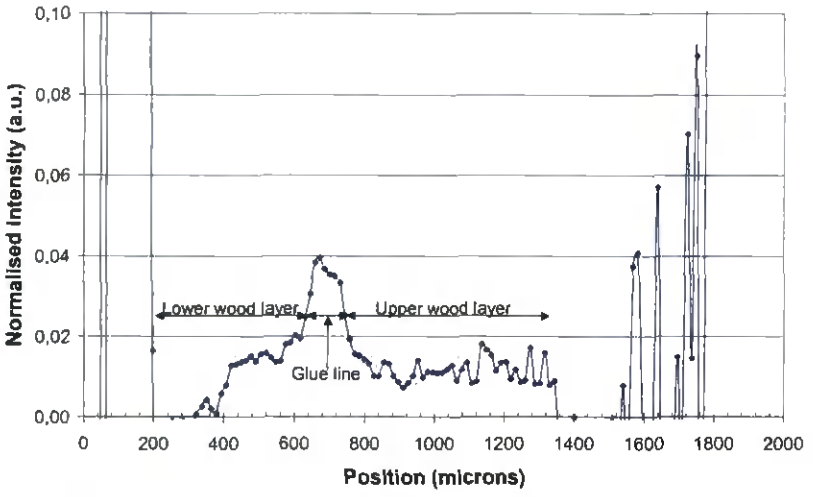

Figure 53. Profile of the glue line without added water taken with 16000 scans.

There is a higher signal intensity between 660 and 730 μm in the profile which is where the glue line is expected to be. The width corresponds also very well with what it should be. This part of the profile appears to 'spread' slightly into the wood as would be expected as the samples were pressed at a pressure of 0.5 MPa during curing. Similar profiles were obtained with other samples. Therefore, it could be the glue line that we have localised. However, it is not yet beyond doubt if it is just a change in wood structure that we are detecting.

5.3.4.2 Water penetration

Example profiles of water ingress into pine wood glued with MUF is shown in figure 54. The radio frequency coil is at 0 μm on the position scale; the marker tape at 250 μm. The sample is positioned between 300 and 1200 μm with the water reservoir beyond this. The glue line is at 800 μm. The original baseline at 0 minutes is shown furthest down in the diagram. Profiles are then shown at different times after the water reservoir was filled. The signal to noise ratio of these profiles gets progressively worse with distance from the coil as this data has been normalised to the elastomer standard to correct for detector sensitivity.

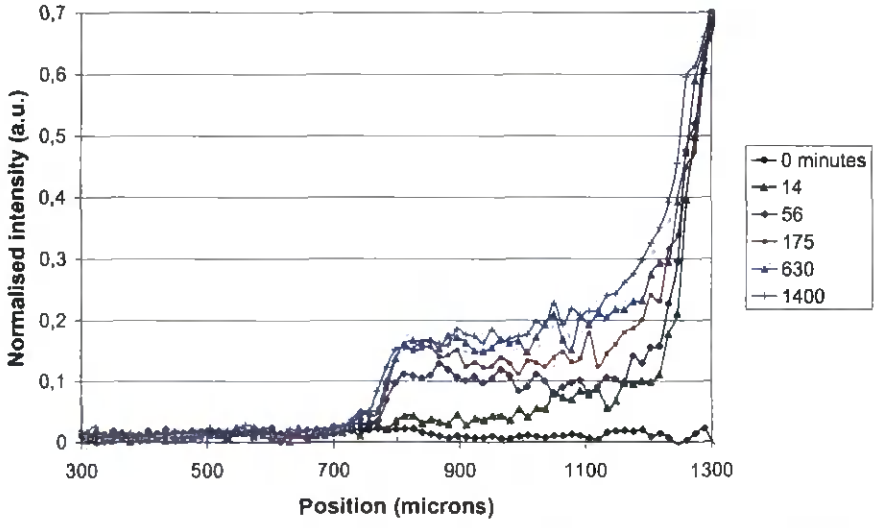

Figure 54. Profiles of water ingress into a sample of pine glued with MUF.

Increased signal due to the water ingress can be seen in the upper wood layer on the profile taken after 14 minutes. The intensity in the upper wood layer continues to increase, in the beginning quickly and thereafter more slowly. An insignificant amount of water penetrates the glue line and reaches the lower layer of wood and the MUF glue thus clearly forms a barrier to water transport for times up to 1400 minutes. There is a similar build up of water in all three samples.

In figure 55, intensity profiles are shown for PRF glue. The glue line is at 600 µm. A build up of water in both wood layers and the glue is shown with an apparent peak in the wood on either side of the glue line at longer ingress times.

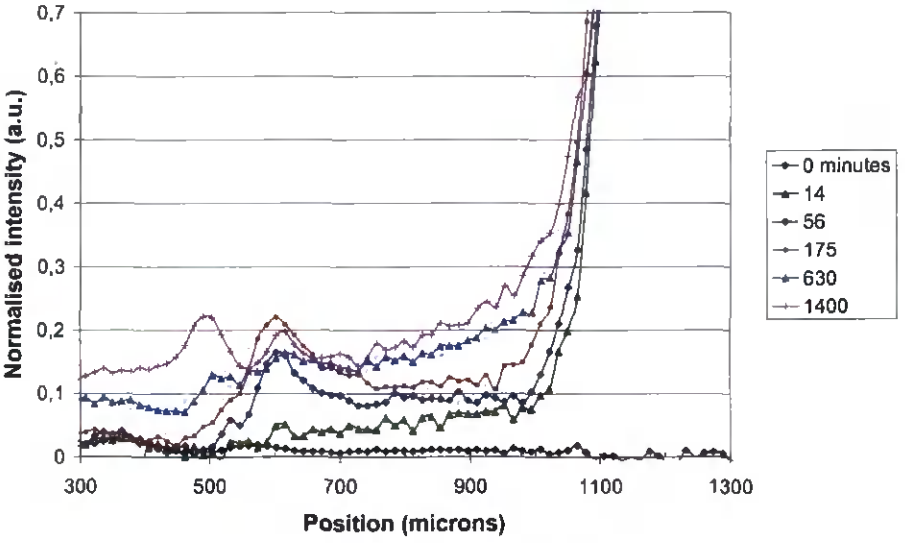

Figure 55. Profiles of water ingress into a sample of pine glued with PRF.

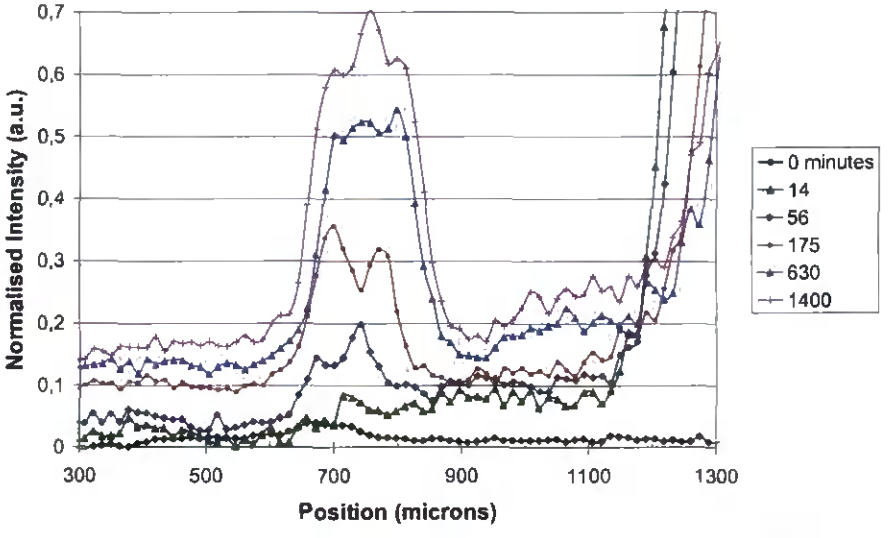

Figure 56. Profiles of water ingress into a sample of pine glued with PVAc without hardener.

Figure 56 shows profiles of water ingress in the PVAc glue. The glue line is at 710 µm. After 1 hour it can be seen that the intensity at the glue line has increased more than in the surrounding wood. This indicates that the glue rehydrates and it can also be seen to

delaminate. The signal originating from the glue line also appears to get progressively wider as does the sample thickness indicated by the position of the water reservoir. The void at the glue line between the two wood layers also appears after 6 hours to fill with water. As the intensity in the lower wood layer appears to be the same as in the upper layer throughout the experiment the glue line appears to be no really obstacle for water diffusion.

5.3.4.3 Comparison of the water increase

In figure 57 the average water absorption of the lower and upper substrate is shown for the different glue types.

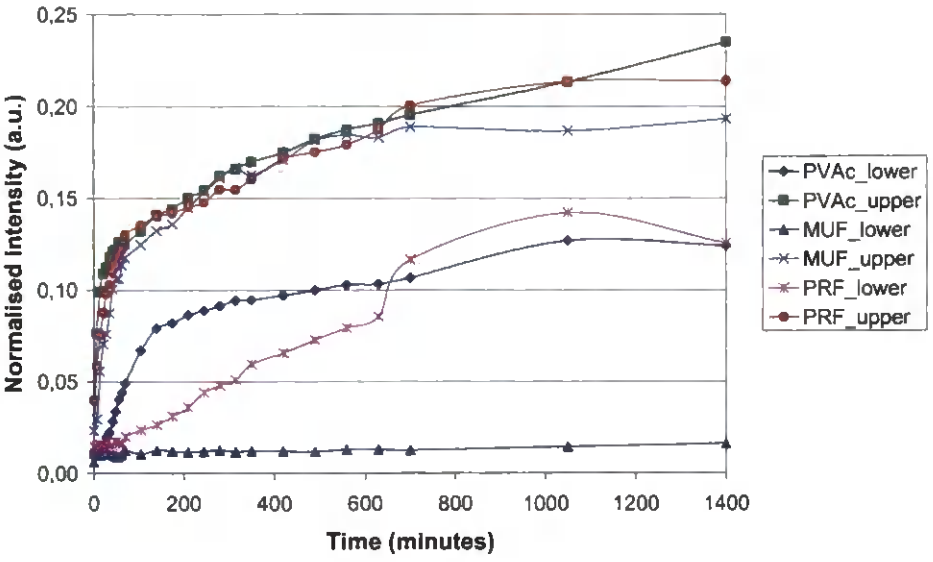

Figure 57. Change in signal intensity with time in the upper and lower wood layer for the different glues. The curves are average values based from the three replicates.

There is no bigger difference in water absorption in the upper wood layer depending on glue type, which could be expected. On the other hand, the water absorption of the lower substrate shows that PVAc glue doesn't allow the water absorption to be as fast as in the upper wood layer but is fairly easy to penetrate for water anyway. The diffusion resistance of PRF glue is situated somewhere between that of the PVAc glue and the MUF glue, but show a somewhat different behaviour. After 10 hours the permeability suddenly increases abruptly for PRF. This might depend on that the structure is loosened up.

After a linear regression of the initial slopes of the curves from the lower wood layer, it can be seen that the diffusion through PVAc is 135 times faster than through MUF and 29 times faster than through PRF, at least during the first 2 hours.

6 Conclusion

6.1 Coatings

The aim with the present work package was to investigate the moisture transport behaviour through different types of coatings. This was done by measuring moisture content profiles during absorption and desorption of water. The moisture content profiles were measured

using MRI. The MRI system used here was developed for non-destructive measurements in planar films. The resolution was in the order of 15 - 20 μm with an field of view of up to 2000 μm.

The results are unique since there are nearly no other published studies available that show moisture content profiles in coating and wood during absorption or desorption of water with such a high resolution.

It is clearly shown that there exists complicated processes at the different interfaces between air, coating and wood as well as in the coatings itself and in the wood substrate which may have great impact on the dynamic processes that takes place when coatings are subjected to moisture and water. Disturbances in these processes may cause large deviations from the intended performances of the systems. Combining the present findings and other research results there is strong reason to focus on the surface-active substances that are essential for producing stable water-borne coating products. Further research is needed to describe the action of water sensitive materials on moisture accumulation in coated wood.

6.2 Drying

The aim with the present work package was to investigate the moisture transport behaviour at a wood surface. This was done by measuring moisture content profiles during drying and conditioning. The moisture content profiles were measured using MRI. The MRI-system used here was developed for non-destructive measurements in planar films. The resolution was between 13 and 21 μm with an field of view of around 300 and 600 μm. This method was used for measurements at the interface between the wood surface and the surrounding air. The results are unique since there are nearly no other published studies available that shows moisture content profiles in a wood surface during drying with such a high resolution. Similar results are though published for other materials, for instance as paper, human skin and food products etc. The results show that the moisture behaviour below the fibre saturation point behaved as expected and according to Fick´s law. At higher moisture contents the behaviour could not be described by existing drying models for wood. New theories such as percolation must be used to describe moisture transport in the capillary phase in a porous media as wood.

6.3 Glues

In the open condition after glue spread, the glue line thickness decreases with 3.0 μm/minute due to evaporation and diffusion into the wood. Measuring only the evaporation effect, the rate of thickness decrease was 1,6 μm/minute and measuring only the diffusion effect, the rate is 0.6 μm/minute. Adding the separate effects does not equal the combined effect. However, more replicates have to be measured in order to draw further conclusions.

In the closed condition after assembly, the rate of thickness decrease was 1.0 μm/minute, which is quite in accordance with double the rate of diffusion into one single substrate.

Further, signs of trapped water in the glue line due to skin formation could be seen and the effect of water adsorption in the cell wall and the subsequent swelling was described.

The decay in intensity of the glue line has been studied with respect to time as a indicator of cure. This shows clear differences between different hardeners and conditions.

Higher storage temperature and increased glue line thickness show a tendency to increase hardening time and increased hardening temperature and increased hardener content tends to decrease hardening time.

It can be concluded that it functions well to monitor the diffusion of liquid water through a hardened glue line with Garfield and also to compare different glues quantitatively.

the water diffusion through PVAc is 135 times faster than through MUF and 29 times faster than through PRF, at least during the first 2 hours.

7 Appendix to Part I

7.1 Appendix A: Optimised parameters for GARField drying experiments

This parameter set is typical of that used for drying studies. However, generally as the water content decreased, water became less mobile etc. it was necessary to increase number of scans. τ could also be shortened.

Setting	Parameter	Value
P90	pulse length, α	1 μs
Dead1	dead time	15 μs
tau	pulse gap, τ	55 or 95 μs
SF	Typical spectrometer frequency	29.3 MHz
DW	dwell time	0.7 or 1.2 μs
SI	Number of points per echo, n	64 or 128
NECH	Number of echoes	16 or 32
NS	Number of scans	256
RB	Receiver bandwidth, δf	1 MHz
G	Gradient strength	17.5 T/m
RD	Repeat duration	0.5 - 2 s

7.2 Apendix B: Optimised parameters for GARField coatings experiments

Setting	Parameter	Value
P90	pulse length, α	1 μs
Dead1	dead time	15 μs
tau	pulse gap, τ	70 μs
SF	Typical spectrometer frequency	29.3 MHz
DW	dwell time	0.7 μs
SI	Number of points per echo, n	128
NECH	Number of echoes	16
NS	Number of scans	1024
RB	Receiver bandwidth, δf	1 MHz
G	Gradient strength	17.5 T/m
RD	Repeat duration	0.5 s

7.3 Appendix C: Optimised parameters for GARField glue line experiments

Setting	Parameter	Value
P90	pulse length, α	1 μs
Dead1	dead time	15 μs
tau	pulse gap, τ	70 μs
SF	Typical spectrometer frequency	29.3 MHz
DW	dwell time	0.7 μs
SI	Number of points per echo, n	128
NECH	Number of echoes	16
NS	Number of scans	512
RB	Receiver bandwidth, δf	1 MHz
G	Gradient strength	17.5 T/m
RD	Repeat duration	1.0 s

7.4 Appendix D: Pixel resolution and Field of View and useful profile length.

The field of view is given by

$$r = \frac{2\pi}{\gamma G t_s}$$

where γ is the (^{1}H) magnetogyric ratio equal to 26.8×10^6 Rads/T. The pixel resolution is given by

$$\delta r = \frac{r}{n}$$

The useful profile length within the field of view is given by the smallest of

(i) the nominal r.f. pulse excitation bandwidth $r_1 = \frac{2\pi}{\alpha\gamma G}$

(ii) the spectrometer receiver or r.f. coil bandwidth, δf, according to $r_2 = \frac{2\pi\delta f}{\gamma G}$

(iii) approximately the r.f. coil radius (here typically $r_2 = 1.5 - 5$ mm).

In the work reported here, factors 1 and 2 were comparable and generally limiting.

Part II

Modelling of surface layer effects: Mass transfer from wood surfaces

1 Introduction

The drying process of wood can be viewed as two resistances in series. The internal resistance is connected to the migration of moisture towards the surface and is described as a diffusion process. The external resistance consists of heat and mass transfer between the surface and the drying air. In order to understand the drying process in whole, both parts have to be considered. Especially in wood drying the interaction between the surface and the air show some peculiar features that deviate from simple standard models.

2 External mass transfer above fibre saturation point (sapwood)

In green sapwood such as pine (*Pinus silvestris*) and spruce (*Picea abies*) the moisture content in the sapwood is high, normally about 130 %. When a sapwood drying process is started, there will thus be a very wet wood surface. The traditional way of describing the evaporation from such a wet surface is illustrated in figure 58.

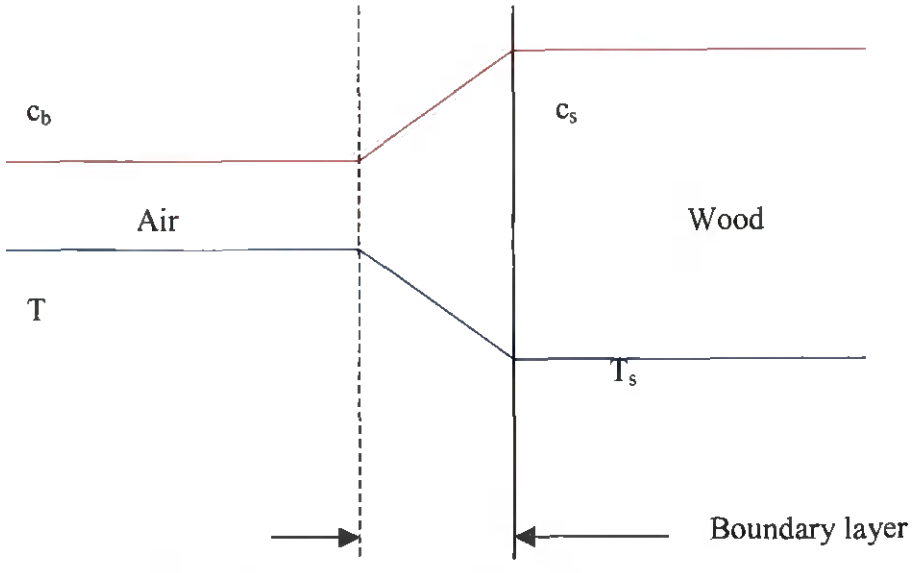

Figure 58. The upper line illustrates the vapor concentration from the bulk air flow, through the boundary layer and into the solid wood. The lower line illustrates the corresponding temperature profile.

The temperature of the bulk drying air is denoted T and the wood surface temperature T_s. The temperature difference $T-T_s$ across the boundary layer is the driving force for the heat flux q to the wood surface

$$q = h(T - T_s) \qquad (1)$$

where h is the heat transfer coefficient. The humidity of the bulk air, expressed as kg H_2O/m^3, is denoted c_b and the humidity of the air in contact with the wood surface is denoted c_s. If this air in contact with the wood surface is in thermodynamic equilibrium with the surface and the surface is wet, then c_s is found from steam tables for pure water at the temperature T_s. The vapor concentration difference c_s-c_b across the boundary layer is the driving force for the moisture flux g from the surface

$$g = h_m(c_s - c_b) \tag{2}$$

where h_m is the mass transfer coefficient. According to the "analogy between heat and mass transfer", we have (at least approximately)

$$h_m = h / C \tag{3}$$

where C is the volumetric specific heat capacity ($J/m^{3o}C$) of the air in the boundary layer.

The moisture concentration in the air (kg H_2O/m^3 air) and the moisture content in wood (kg H_2O/m^3 wood) are of course quite different in magnitude. In order to simplify the presentation in figure 58, the moisture concentration within the wood is also given as kg H_2O/m^3air, i.e. moisture concentration in the gas phase, in equilibrium with the local moisture content. This gives a continuous line in figure 58. As the moisture content is above FSP in this case, a horizontal line is obtained inside the wood, although the moisture content is not necessarily constant.

For constant drying conditions – after an initial transient period – an equilibrium between the heat flux to the surface and the heat consumed by the evaporation is attained, i.e. a constant drying rate is found as long as the surface is wet. This by definition corresponds to $T_s = T_w$ = wet bulb temperature. A completely wet surface will thus give a constant drying rate, and this is found in practice for many materials. This includes wood, but in that case the constant rate period is often not very clearly seen. It should also be reminded that a constant drying rate does not necessarily prove that we have a "wet surface" situation. There could be other mechanisms that give a constant (or nearly constant) drying rate, but then normally below the rate given by Eq.(2) for the wet surface case.

There is, however, a multitude of experimental results that indicate that the situation illustrated by figure 58 is not always relevant for wooden surfaces – not even for very wet sapwood. The simplest indication is the fact that the wood temperature normally arises above the wet bulb temperature very soon after the drying process is started. Another indication is a non-constant drying rate. At the same time measurements of the moisture content profile inside the wood sample give rather flat profiles. Direct measurement of the surface moisture content is very difficult, but an extrapolation of these profiles towards the surface can often give values far above FSP (Wiberg 2001), indicating a wet surface. This also is verified in the high resolution measurements in Rosenkilde *et al* 2002a,b. These indications can also be viewed as *apparent* deviations from the analogy between heat and mass transfer (Eq.(3)).

What are then the physical reasons behind these findings that contradict the situation presented in figure 58? It has been suggested that the surface is not completely wet, but contains "dry spots" that decrease the effective area for mass transfer, but not the area for heat transfer. However, it has been shown that dry spots that are small compared to the boundary layer thickness will not influence the transfer rate very much. It should further be noted that even if there is no free water at the dry spots, there is still a lot of bound water, giving an equilibrium air moisture concentration not very much below the value corresponding to free water. Thus "dry spots" should only have a marginal effect on the interaction between the wood surface and the drying air.

The presently most widely accepted explanation of the apparent deviation from the analogy between heat and mass transfer is the "dry shell" concept. This is explained in more detail by figure 59.

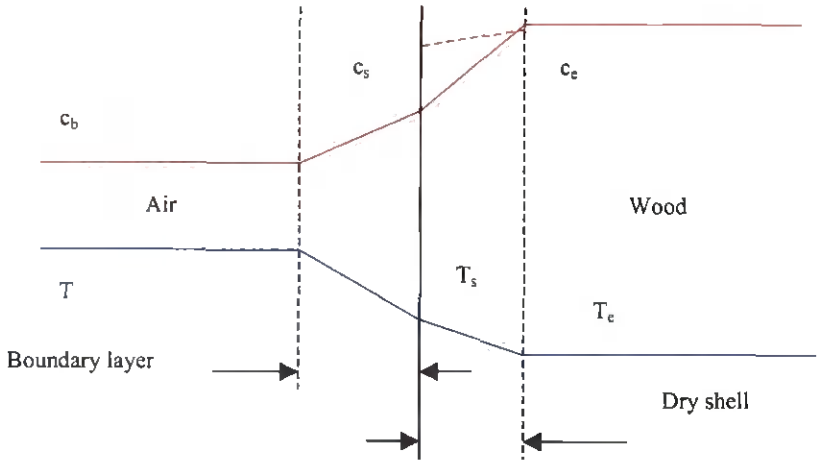

Figure 59. Vapor concentration and temperature profiles across the wood surface according to the "dry shell" concept.

The air side part is unchanged compared to figure 58. Within the wood a "wet line" has developed, Keey et al[40]. This line and the surface define a "dry shell" where there is no free water. To the right of the wet line there is still free water and moisture evaporation is assumed to be concentrated to the wet line, i.e. an evaporation front. This dry shell situation is now analyzed based on measurements done in a project reported in (Wiberg 2001 and Wiberg et al 2000).

Measurement raw data has kindly been supplied by (Morén et al 2001). Temperatures measured in test A are presented in figure 60. It is seen that the temperature in the inner part of the sample is almost from the beginning higher than the wet bulb temperature, but below the surface temperature as in figure 59. The wood sample was weighed during drying and the drying rate is thus known. Further details regarding the test method are found in (Wiberg 2001).

[40] Keey, R.B., Langrish, T.A.G., Walker, J.C.F., 2000, Kiln-Drying of Lumber, Springer-Verlag, Germany.

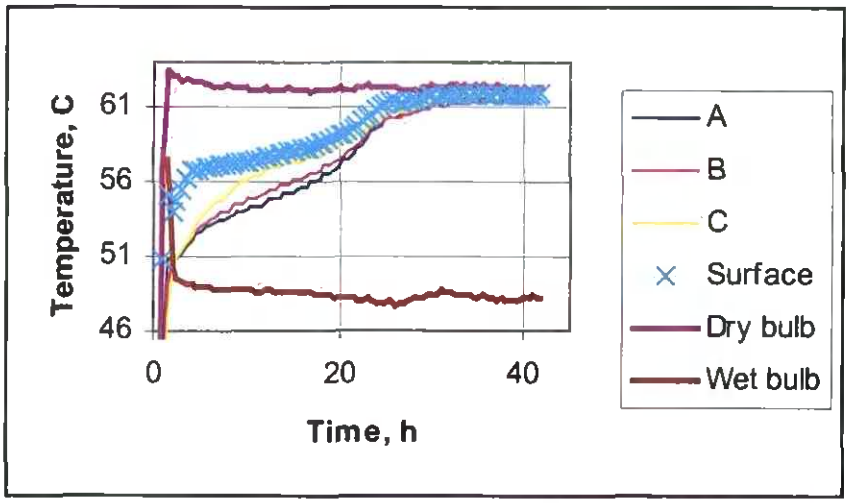

Figure 60. Temperatures measured in drying test A. Letters A-C stand for points at different depths inside the wood sample.

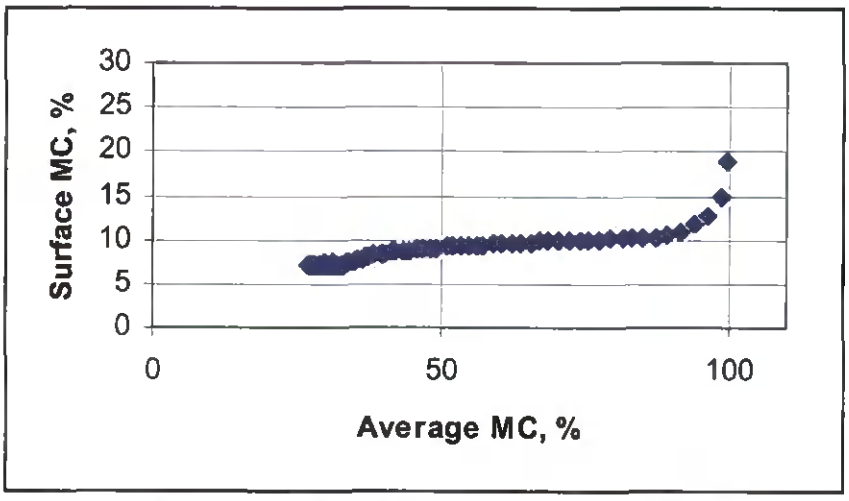

Figure 61. Calculated surface moisture content as a function of the average sample moisture content. (Uncorrected surface temperature.)

If the rather small changes in wood temperature, the heat of sorption, etc, are neglected, the drying rate combined with the heat of evaporation gives the heat flux to the surface and from the measured surface and air temperatures a heat transfer coefficient is found from Eq.(1). The result was about 100 W/m^2K for test A (and about the same for other tests also). This is a very high value, but it should be noted that the air velocity was high, 6 m/s, with extra turbulence generated by experimental devices. However, the surface temperature is not very reliable due to the measurement method used and this will be discussed later. From the heat transfer coefficient, the mass transfer coefficient is found from Eq.(3) and as the bulk air flow humidity is known, the air humidity close to the surface, c_s, can be calculated from Eq.(2). Assuming equilibrium at the surface, the surface moisture content can be calculated from the sorption curve corresponding to the measured surface temperature. The result is presented in figure 61.

As can be seen the surface moisture content has dropped below FSP almost immediately, despite a high average sample moisture content, and stays fairly constant for a long time.

Now, as we know the surface moisture content, the average heat conductivity of the dry shell can be estimated and thus the distance to the evaporation front (shell thickness) is further obtained from the known heat flux and internal wood temperature. The result is seen in figure 62. After about 24 h drying time, strong fluctuations in the calculated shell thickness appear as a result of measurement inaccuracies. Further the shell thickness starts to increase above 2 mm, which is the depth of the internal wood temperature measurement point used, so the calculation method fails for longer drying times. The obtained shell thickness starts at about 1,6 mm and increases gradually. A similar calculation, using the same data set, is presented in (Wiberg 2001) and yields a thickness around 1 mm for tests A-G.

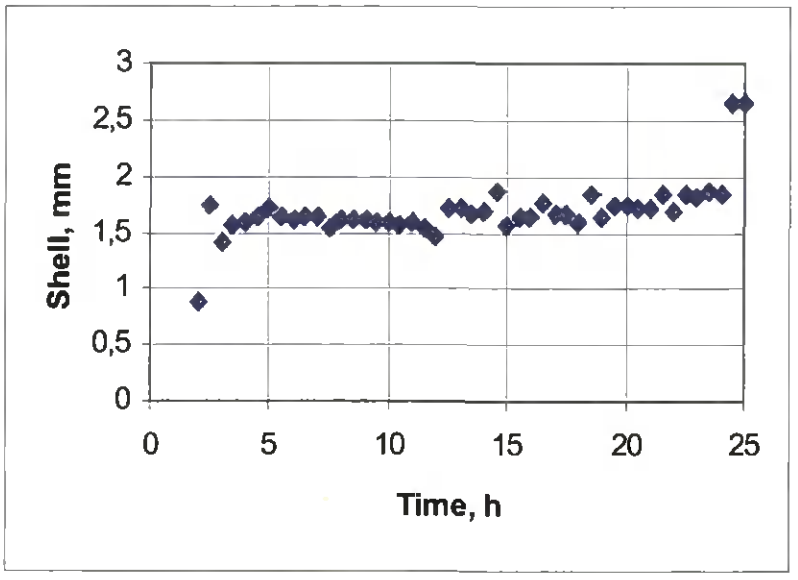

Figure 62. Calculated dry shell thickness as a function of time. (Uncorrected surface temperature.)

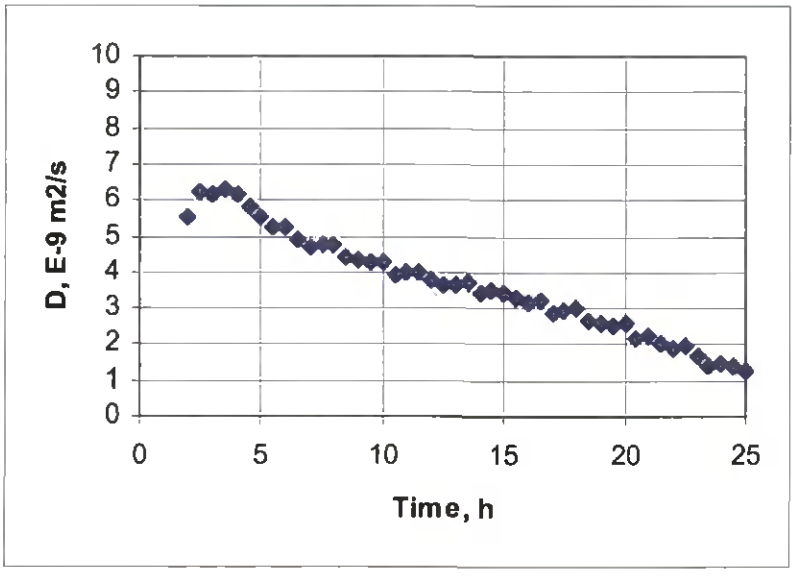

Figure 63. Calculated average diffusion coefficient for the dry shell. (Uncorrected surface temperature.)

As the thickness of the shell and its state thus has been established, an average moisture diffusion coefficient for the shell can be found from the known moisture flux. The result is given in figure 63. The result differs clearly from what was expected. First, a rather constant value was expected as the moisture content level within the shell remains rather constant (surface moisture content.... FSP). Second, the expected level for pine sapwood is about $1 \cdot 10^{-9}$ m^2/s, Rosenkilde et al[41]. There is thus obviously an error somewhere in the analysis.

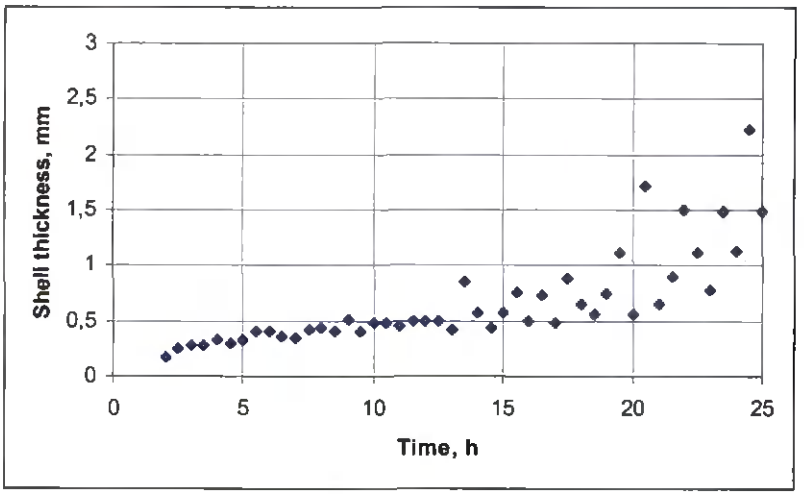

Figure 64. Calculated dry shell thickness as a function of time, with corrected surface temperature.

The surface temperature is a very essential part in the above analysis. As already mentioned, this measurement is not very reliable. In connection with these drying tests an attempt was made Morén[42] to measure the heat transfer coefficient by replacing the wood sample by pure water in an open box, and measuring the weight loss. The result was 63...67 W/m^2K, i.e. lower than the value (100 W/m^2K) based on the measured wood surface temperature. Using this heat transfer coefficient a "new" surface temperature can be calculated and the above analysis repeated with this new value. It is then found that the diffusion coefficient, instead of decreasing from about $6 \cdot 10^{-9}$ to $1 \cdot 10^{-9}$ m^2/s (figure 63.), will decrease from $2 \cdot 10^{-9}$ to $0{,}7 \cdot 10^{-9}$ m^2/s, which is much closer to the expected level. As the calculation obviously is sensitive to errors in the surface temperature, another approach is used. For each point the surface temperature is determined in such a way that the calculated diffusion coefficient for the dry shell equals the expected value, in this case given by Rosenkilde et al[41]. The result obtained in this way for the shell thickness is seen in figure 64.

The result in (figure 64) is more logical than above (figure 62), as the shell thickness starts from zero and then gradually increases. Although the result seen in figure 64 is certainly inaccurate, it is believed that it reflects the situation in the wood surface layer correctly and that it constitutes a strong indication that the mechanisms illustrated in figure 59 are correct.

---

[41] Rosenkilde, A., Arfvidsson, J., 1997, Measurement and evaluation of moisture transport coefficients during drying of wood, Holzforschung 51,372-380.

[42] Morén, T.J., Sehlstedt-Persson, S.M.B., 2001, Personal communication.

3 Dry shell – direct measurements

Direct observation of the surface moisture content and the dry shell is very difficult. A CT-scanning procedure reported in Wiberg[43] showed clearly a high moisture content level near the surface and indicated a steep drop in the outermost part close to the surface. A detailed picture of this dry shell was however not achieved due to insufficient spatial resolution.

A dry shell was clearly seen in experiments reported in Tremblay *et al* [44] where five slices 0,38 mm thick were removed from the surface and the moisture content measured. A steep moisture content gradient was seen within a shell with a thickness of about 2 mm. When the average moisture content drops below FSP the dividing line seems to disappear and a smooth moisture content profile is obtained.

Recently high-resolution non-destructive measurements using an MRI technique have been used for determination of moisture conteent profiles (Part I, section 0) within a 0,3 mm thick surface layer (Rosenkilde *et al* [45,46,47]). Initially an about 0,09 mm thick shell seems to develop, which may be linked to the fiber structure. The moisture content gradient is continuously extremely steep, as the shell becomes thicker. The shell thickness development cannot be generally determined in this case, as it exceeds 0,3 mm rather soon.

These three examples are in good general agreement with the calculations above and with the final result as represented by figure 67.

4 External Mass Transfer Below Fsp

Below FSP – with no free water present – the traditional way to describe moisture evaporation from a wooden surface is similar to figure 58. In this case, however, c_s is not the vapor concentration above a free water surface, but the concentration given by the sorption curve for the corresponding surface moisture content and temperature. The c-curve inside the wood is also no longer horizontal as in figure 58. Based on experimental evidence, however, there are strong indications – similar to the ones in the wet sapwood case – that this description is not always valid for wooden surfaces. Some of these deviations where summarized by Salin[48]. More recently Hukka[49], Hukka et al[50] and Tremblay *et al* [44]) have reported similar results. In

---

[43] Wiberg, P., 2001, X-ray CT-scanning of wood during drying, Doctoral thesis, Luleå University of Technology.

[44] Tremblay, C., Cloutier, A., Fortin, Y., 2000, Experimental determination of the convective heat and mass transfer coefficients for wood drying, Wood Science and Technology 34,253-276.

[45] Rosenkilde, A. 2002. Moisture content profiles and surface phenomena during drying of wood. Doctoral thesis, KTH-Royal Institute of Technology, TRITA-BYMA 2002:4.

[46] Rosenkilde, A., J-P Gorce and A. Barry. 2003. Measurement of moisture content profiles during drying of scots pine using magnetic resonance imaging. Accepted for publication in Holzforschung.

[47] Rosenkilde, A., Glover, P., 2002, High resolution measurement of the surface layer moisture content during drying of wood using a novel Magnetic Resonance Imaging technique. Holzforschung 56:312-317.

[48] Salin, J-G., , Mass transfer from wooden surfaces, 10th International Drying Symposium, Kraków, Poland, July 30 – Aug. 2. 1996

[49] Hukka, A., 1999, The effective diffusion coefficient and mass transfer coefficient of Nordic softwoods as calculated from direct drying experiments, Holzforschung 53,534-540.

[50] Hukka, A., Oksanen, O., 1999, Convective mass transfer coefficient at wooden surface in jet drying of veneer, Holzforschung 53,204-208.

all these cases the mass transfer from the surface is slower than expected. What are then the reasons for such findings?

A low mass flux has to mean that c_s in Eq.(2) is lower than expected. If thermodynamic equilibrium is assumed at the surface, then surface moisture content has to be lower than expected also. The surface moisture content is extremely difficult to measure in a dynamic situation, like the drying process. Extrapolation of the internal moisture profile towards the surface is one possibility, and that is actually – in a way – the method used for instance by Hukka. It could be argued that the sorption curve, used to determine the connection between c_s and surface moisture content, is perhaps incorrect. Especially if the hysteresis effect is taken into account, this could at least partly explain the "gap" between surface moisture content and vapor concentration close to the surface. But if the very low c_s values found by Hukka at higher temperatures – where the hysteresis effect should be smaller – are considered, then this alternative does not seem to give a complete explanation.

It has in this discussion been assumed that there is a local thermodynamic equilibrium between the wood and the gas phase, both at the surface and in the interior parts. If this is not the case, that could be an explanation to the observed phenomena. It has traditionally been taken for granted that equilibrium is attained due to the huge (fiber level) transfer area between the gas and the bound phases. However, as has theoretically been shown by (Salin[48] and Cunningham[51]), even a rather limited deviation from the equilibrium will produce an essential overall effect.

If it, based on experimental results, is accepted that there is an additional "surface resistance" that affects the drying rate, then this very same phenomenon has to influence the "dry shell" behavior in the wet sapwood case too, as the moisture content is below FSP within this shell. This regardless of the explanation behind this extra surface resistance. In such a case the description given in connection with figure 59 is not fully correct, as equilibrium was assumed within the dry shell. In that case the dotted line within the shell corresponds to the equilibrium c-value calculated from the bound water content.

5 Modelling

The "dry shell" concept seems to give a reasonable explanation to the observed drying behavior above FSP. Modeling of this behavior requires that the shell thickness development can be predicted. Probably the "wet line" withdrawal has to be viewed as a pore network problem, strongly linked to capillary phenomena. An excellent review of such problems and recent advances is found in (Prat[52]).

First, it has to be realized that the wet line is not a well-defined plane, but a complex surface of a fractal dimension between 2 and 3. The local position is determined by the "throats" in the network and their size distribution. Evaporation mainly takes place from throats closest to the surface, but water withdrawal is concentrated to the widest openings further in. The wet line moves because dry areas in the form of microscopic "fingers" or "trees" penetrate into the fiber network. The average position of the wet line thus probably defines a thicker shell than the "effective" shell thickness calculated above (figure 64).

---

[51] Cunningham, M.J., 1995, A model to explain "anomalous" moisture sorption in wood under step function driving forces, Wood and Fiber Science 27(3),265-277.

[52] Recent advances in pore-scale models for drying of porous media. 12th International Drying Symposium, Noordwijkerhout, The Netherlands, Aug. 28-31 2000

Measurements by Wiberg[43] and Rosenkilde[45] indicate that the moisture content profile is almost horizontal in the inner wet part, i.e. the free water movement resistance is small. Thus the wet line position should be mainly determined by network geometry and by the total amount of remaining free water. External conditions and for instance the wood temperature should have a smaller influence. On the other hand, the temperature seems to have an effect on non-equilibrium phenomena in areas below FSP (Hukka, Hukka et al 1999 and Laurila[53]).

As long as these phenomena cannot be modelled in a detailed way, the only practical solution is to insert "correction factors" into the traditional models. The easiest way to introduce such a correction is to alter the mass transfer coefficient value. This seems to be the solution predominantly employed in existing wood drying simulation models. It has to be stressed that this creates an *apparent* mass transfer coefficient, which does not reflect the real situation within the air side boundary layer.

6 Conclusion

The mass transfer from wooden surfaces during drying has been investigated. Based on theoretical and experimental considerations the development of a dry shell at the surface of a wet piece of wood seems to explain the observed overall behaviour. The shell thickness development has been calculated from previously published experimental data. The importance of reliable surface temperature measurements in that context is stressed. For drying clearly below FSP there seems to be a similar situation with lower transfer rates than expected. It is pointed out that these phenomena should influence the behaviour above FSP as the shell itself is below FSP. Finally the possibilities to model these surface phenomena are briefly discussed.

[53] 1993, Evaporation from wooden surfaces. (In Finnish). M.Sc.(Eng.) Thesis, Lappeenranta University of Technology, Finland.

Part III

Moisture sensors for industrial kilns – A new kiln control system

1. Introduction

Timber drying is one of the most important processes when manufacturing sawn timber products. The drying process influences energy consumption, environment, deformations, surface checking, discoloration and hence, the product quality and the manufacturing costs. Research in this field is of great importance for the wood industry since the industrial drying process always needs to be improved as market demands increase, and new wood products are developed. The main aim with this work was to improve the industrial drying process by incorporating new knowledge based on research in a kiln control system which then will make a much more efficient drying process. The breakthrough in this project is that a new kiln control system with an incorporated drying model has been developed. And for the first time this model describes the behaviour at the wood-air interface which further has been verified by measurements reported in Part I.

2. Development of moisture sensor

The new moisture sensor was developed with the aim to get a feedback from the timber during drying. The signal from the sensor is meant to be used in the control system for controlling the drying climate at the later part of the drying period when the moisture content in the wood is below the fibre saturation point, FSP. To improve easy handling of the sensor it was designed with wireless communication with the controlling computer in the kiln control system. This is very important for the kiln operators that could have a lot of kiln to work with, if it is not easy to use it would not be used as it was meant. Figure 65 below shows the sensor with the transmitter in a kiln stack of timber.

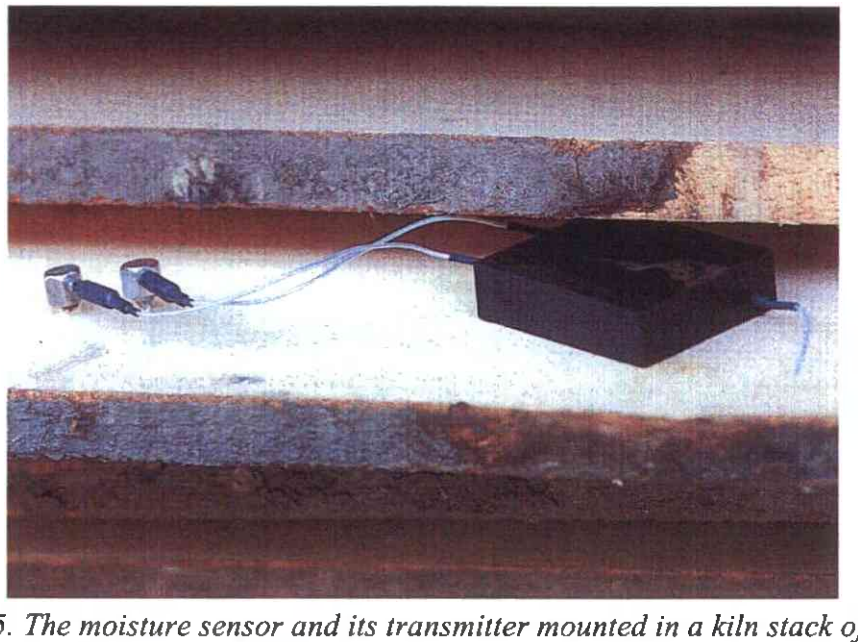

Figure 65. The moisture sensor and its transmitter mounted in a kiln stack of timber.

The biggest problem with developing the moisture sensor was to get the electronics stable and lasting in the kiln climate. There has been a lot of effort in making the sensor water and climate proof, still there is more to be done if the sensor should be used at higher temperatures (above 70 °C) combined with high relative humidity.

The sensor and transmitter can also be used in other applications when the moisture content in wood is needed to be monitored, for instance it can be used for looking at water uptake during storage and transportation to the end customer. This is a very important bit in the quality assurance process of wood products.

3. Development of kiln control system

The kiln control system Optor has been developed with the aim to improve the efficiency of the drying process concerning capacity, energy consumption and wood quality. The idea in this work was to incorporate new knowledge based on research into the control system by incorporating the drying model from Part II, (Salin[54]). The main new function in the control system is that is now possible to simulate the drying process in advance and get an advanced estimation of the drying results such as drying time, moisture content, stresses, checks and moisture content gradient. With this information the drying schedule can be adjusted or not. It is also possible to simulate continually during drying which will make it possible to change the schedule during the drying period if for instance the energy from the boiler is not enough. This happens often at a sawmill when several kilns start on the same day or if there is problems with wet waste fuel to the boiler. Figure 66 show logged climate and other parameters such as ventilation, power etc.

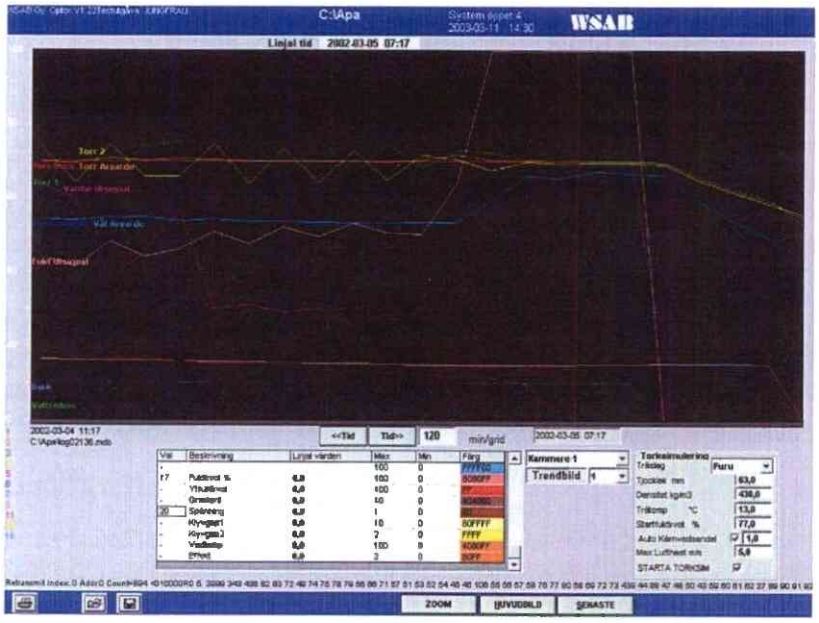

Figure 66. Logged values in the new kiln control system Optor from WSAB.

With the simulation model in Optor it is also possible to make a simulation on the results from a dried batch. The system then uses the real logged schedule and simulates the drying results. This can be used when the drying results needs to be analysed because of for instance

[54] Salin, J-G., 1996, Mass transfer from wooden surfaces, 10th International Drying Symposium, Kraków, Poland, July 30 – Aug. 2.

wrong moisture content or to much surface checking. This is a complete new function, which could save a lot of timber from being downgraded due to bad quality. Figure 67 shows the result from a simulation of a schedule before drying. The drying period is divided into five different phases, heating up, drying, cooling down, conditioning and cooling down. All these five phases can have different parameters for controlling the kiln since the system has to be trimmed to work properly in each phase. It is not possible to use the same controlling parameters in both heating up phase and drying. The heating up phase is a much faster process where the control system has to react very quickly compared to the drying phase where the system has to be stable without fluctuations in the climate.

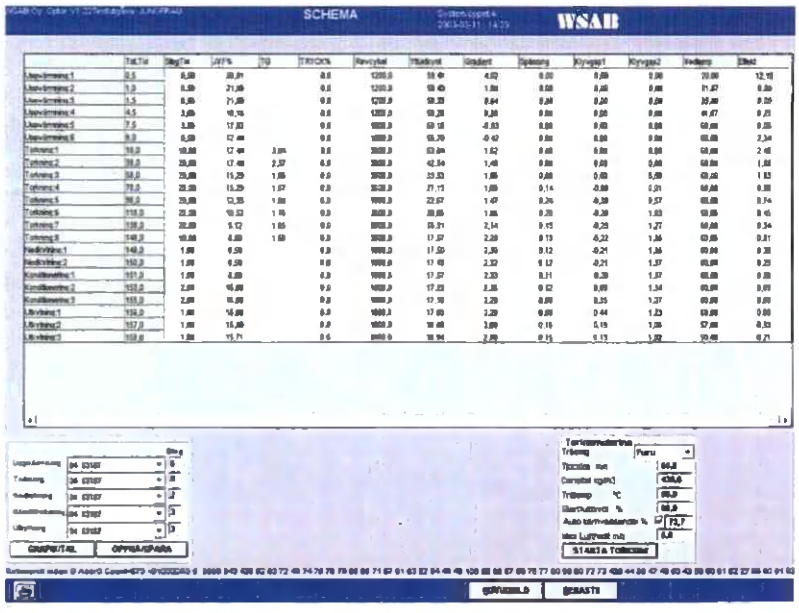

Figure 67. Drying schedule with simulated results in the control system Optor from WSAB.

4. Conclusion

The first version of the control system Optor is now available on the market. The main difference between this new system and older versions is that it now is possible to predict the drying results in advance and it is also possible to analyse a dried batch and use the logged climate for simulation, this is an advanced tool which will help the kiln operators in their effort to dry the wood efficient with good quality which meets the demands from the end customers.

The moisture sensor is also available on the market and it is working well in kilns with lower temperatures, below 70 °C, and not saturated climates. The sensor can also be used for monitoring the wood moisture content in a batch during storage at the sawmill before transport to the end customer.

Acknowledgements

The authors thank Dr Paul Glover, Dr Amanda Barry, Dr Jean-Philippe Gorce and Mr Keith Proctor for much help with this project at the University of Surrey. Paul began the project as project co-ordinator but moved to a new position during the first year. Nonetheless, he contributed much, particularly to the instrumentation and remained interested throughout. Dr

Barry was employed for a short while as a post-doctoral researcher on the project while Jean-Philippe, although employed on another programme was often able to contribute know-how especially with regard to data processing. Keith provided the project with technical support and built many of the probes and ancillary equipment.

PJM thanks Dr Lynn Boniface and Mr Joe Flynn at the University of Surrey and Mrs Gunilla Rodfors at AB Traetek for much help with project administration and reporting.

Detta digitala dokument
skapades med anslag från

**Stiftelsen Nils och Dorthi
Troëdssons forskningsfond**

Trätek

INSTITUTET FÖR TRÄTEKNISK FORSKNING

Box 5609, 114 86 STOCKHOLM
Besöksadress: Drottning Kristinas väg 67
Telefon: 08-762 18 00
Telefax: 08-762 18 01

Vidéum Science Park, 351 96 VÄXJÖ
Besöksadress: Lückligs plats 1
Telefon: 0470-59 97 00
Telefax: 0470-59 97 01

Skeria 2, 931 77 SKELLEF
Besöksadress: Laboratorgrä
Telefon: 0910-28 56 00
Telefax: 0910-28 56 01